Sabina Sušnik, BSc

Analysis of Thermo-Mechanical Deformations of Thin Films under High Heating Rates

MASTER'S THESIS

to achieve the university degree of

Diplom-Ingenieurin

Master's degree programme:

Technical Physics

submitted to

Graz University of Technology

Supervisor

Assoc.Prof. Dipl.-Phys. Dr.rer.nat., Wolfgang Sprengel

Institute of Materials Physics

In cooperation with

KAI Kompetenzzentrum für Automobil- und Industrieelektronik GmbH

Graz, february 2021

AFFIDAVIT

I declare that I have authored this thesis independently, that I have not used other than the declared sources/resources, and that I have explicitly indicated all material which has been quoted either literally or by content from the sources used. The text document uploaded to TUGRAZonline is identical to the present master's thesis.

Date, Signature

Kurzfassung

Das Ziel dieser Arbeit ist die Untersuchung des thermo-mechanischen Deformationsverhaltens dünner Schichten auf Si-Substraten unter hohen Heizraten (bis zu $10^4\,\mathrm{K\,s^{-1}}$). Die Krümmungsmessungen von speziellen Chips werden mit einem Setup, das für schnelle Heizpulse designed wurde, durchgeführt. Die verwendete Methode, welche bereits von *T. Islam* beschrieben wurde, basiert auf Laser Doppler Vibrometrie und wurde im Zuge dieser Arbeit angepasst und verbessert. Sie ermöglicht die Geschwindigkeits- bzw. Abstandsmessung an mehreren Punkten an der Oberfläche eines aktiv beheizten Halbleiter-Chips während mehrerer Heizpulse. Im Vergleich zu den von *T. Islam* durchgeführten Messungen, wurden zur Erstellung dieser Arbeit kleinere Proben verwendet, wodurch das Signal-Stör-Verhältnis durch Optimierung der Messparameter verbessert werden musste. Zusätzlich wurden die Proben gedünnt, um die Verbiegung während der Heizpulse zu erhöhen.
Ein Datenverarbeitungsprogramm, das aus den erhaltenen Daten die Krümmung über die Zeit berechnet, wurde geschrieben. In Kombination mit der gemessenen Temperatur über die Zeit, liefert es die Krümmungs-Temperatur-Beziehung.

Mit konventionellen Geräten zur Krümmungsmessung können nur verhältnismäßig geringe Heizraten (bis zu ca. $2.5\,\mathrm{K\,s^{-1}}$) erreicht werden. Mit dem Aufbau, der das Laser Doppler Vibrometer und die Möglichkeit zum aktiven Heizen beinhaltet, werden Heizraten bis zu $10^4\,\mathrm{K\,s^{-1}}$ möglich. Der große Unterschied in den Heizraten führt zu sehr unterschiedlichen Krümmungs-Temperatur-Beziehungen. Da die Heizraten im Falle einer Überlastung sehr hoch sind, erlaubt der in dieser Arbeit präsentierte Aufbau, die Messung der Krümmungs-Temperatur-Beziehung unter andwendugsrelevanten Bedingungen. Der bemerkungswerteste Unterschied zu Experimenten, die mit niedrigen Heizarten durchgeführt werden, ist, dass das linear-elastische Verhalten bis hin zu weitaus höheren Temperaturen beobachtet werden kann (320 °C bei hohen Heizraten, verglichen mit 120 °C bei niedrigen Heizraten).

Abstract

The aim of this master thesis is to study the thermo-mechanical deformation behaviour of thin films on Si substrates under high heating rates (up to $10^4\,\mathrm{K\,s^{-1}}$). The measurements are performed with an experimental setup for curvature measurements of specially designed chips during rapid heating pulses. The setup is based on laser Doppler vibrometry, as described by *T. Islam*, but has been adapted and improved within this thesis. In particular, it allows the measurement of the velocity/displacement at several points on the surface of an actively heated semiconductor chip during several heating pulses. In comparison to the measurements performed by *T. Islam*, smaller samples were used within this thesis meaning that the signal-to-noise-ratio had to be improved by optimizing the measurement parameters. Additionally, the samples were thinned to increase the bow during a heating pulse.
A data processing program for deriving the curvature vs. time from the obtained data has been developed. Combined with the measured temperature vs. time the curvature-temperature relation is obtained.

Conventional curvature setups can only perform measurements with comparatively low heating rates (up to roughly $2.5\,\mathrm{K\,s^{-1}}$). With the measurement setup including a laser Doppler vibrometer and the possibility of active heating, heating rates up to $10^4\,\mathrm{K\,s^{-1}}$ become possible. The big difference in the heating rates causes very different curvature-temperature relations. As the heating rate in case of an overload event is very high, the setup presented in this thesis allows measuring the curvature-temperature relation at application relevant heating conditions. The most remarkable difference to experiments performed at lower heating rates is that linear-elastic behaviour can be observed until much higher temperatures (320 °C at high heating rates compared to 120 °C at low heating rates).

Contents

1 Introduction

Power semiconductor chips are used in many electronic systems, e.g., in the automotive truck or sensing application. Their main purpose is to control the power densities, which can range from mega- to microwatts. [1]
In general, a semiconductor chip consists of structured layers of different materials: semiconducting substrates, dielectrics used as insulating layers and power metallizations. These materials do not only have different electrical properties but also distinguish in terms of their coefficients of thermal expansion (CTE). This means that changes in temperature lead to different thermal expansions of the respective materials resulting in stress in the layers and shear at the interfaces. On a macroscopic scale such stresses become apparent as the whole chip bends.

In case of an overload event in such a chip, high power (peak power may reach several kW) may be generated within a few microseconds. Throughout its operational lifetime, the device has to withstand many of those events, during which a big part of the power is dissipated as heat. [2] As a consequence of the different thermal expansions, the chip bends. It is important to understand, what happens during those temperature cycles, as this strongly influences the lifetime.

Wafer curvature is a technique that was developed for measuring the temporal evolution of bow of whole wafers while being subjected to predefined thermal recipes. Wafer curvature tools can conceptually be subdivided into a heating system and a system for the curvature measurements. In most of the wafer curvature tools the wafer is located in a chamber, which as a whole is heated, e.g., by means of electrical heating or infrared lamps. With this passive heating possibility only low heating rates (less than $1\,\mathrm{K\,s^{-1}}$) can be achieved. To increase the heating rates (up to the range of $2.5\,\mathrm{K\,s^{-1}}$), the tools have been adapted by reducing the size of the heated volumes. The heating system was changed to a heating stage instead of a whole oven. As a consequence only measurements on smaller samples such as, for example, wafer pieces are possible with these adapted systems.
By changing the heating possibilities from the passive methods mentioned above to active heating via specially designed chips (so-called "polyheaters"), shorter pulses and thus higher heating rates can be achieved. The usage of polyheaters together with a special setup for actuating them enables heating rates up to $10^8\,\mathrm{K\,s^{-1}}$ reaching temperatures above $400\,^\circ\mathrm{C}$, which is close to conditions that may occur in a power semiconductor during an overload event. [3] But as the chips are usually very small (roughly $2\,\mathrm{mm} \times 3\,\mathrm{mm}$), they can not be measured with standard wafer curvature systems. Also measurements with adapted wafer curvature systems become impossible for such samples as their scan times are much longer than the duration of a pulse.

The aim of this master thesis is to expand a currently existing experimental setup to allow curvature measurements of polyheaters at very high heating rates (up to $10^4\,\mathrm{K\,s^{-1}}$). For such fast curvature measurements a method based on laser Doppler vibrometry was

chosen, which has already been described by *T. Islam.* [4] Nevertheless the measurement procedure had to be improved and a code for the analysis of the measurement data had to be developed.

The polyheaters examined in the past had an aluminum metallization on top, but it was exchanged by copper. The new types of polyheaters have so far never been successfully investigated at high heating rates. At the end of the thesis, the results of the experiments should thus provide data for the calibration of a thermo-mechanical model of the power metallization layer in dependence of the temperature.

2 About Thin Film Deformation and Curvature Measurements

2.1 Fatigue of Metals

In general fatigue of metals is the consequence of repeated mechanical or thermal loading. Although for each cycle the maximum load is lower than the breaking load, over a very large number of cycles subtle gradual microstructural degradation accumulates causing fatigue and eventually break down of the specimem tested. [5]
In semiconductor chips, pulses during which the chips are heated cause thermomechanical fatigue. Figure 1 illustrates the mechanical behaviour of a bilayer system representing a substrate with a metallization on top upon variation in temperature.

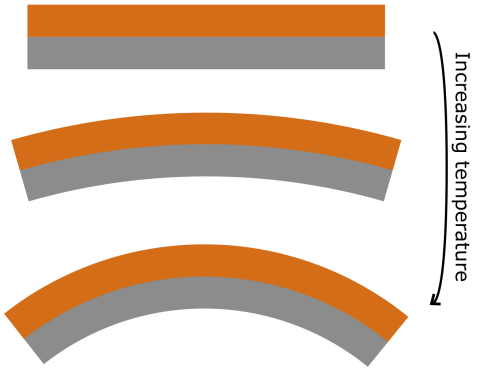

Figure 1: Schematics showing the thermally induced bow of a bilayer system.
(substrate (grey) = lower CTE, metallization (orange) = higher CTE)

As already mentioned in sec. 1, a temperature change causes the bending of the system as the materials have different CTEs. Due to the metallization being attached to the substrate, the bending leads to strains and stresses. Depending on the applied strain and temperature combination different deformation mechanisms explained in the following, may occur in the material. [6]

2.1.1 Elastic Deformations

An elastic deformation is a reversible deformation meaning that a material reaches its initial form after having been exposed to an external force. While the force is applied, the atomic lattice is deformed, e.g. stretched, but the atoms do not permanently change their position. [7]
A measure for the stiffness and thus also for the ability of a material to deform elastically is the so called Young's modulus. It also is the coefficient describing the relation between stress and strain in the elastic regime, which can be different for different orientations of a material.

2.1.2 Plasticity

At low temperatures and high stresses plastic deformation occurs meaning that a material is deformed irreversibly. The most important causes for plasticity to occur are dislocation nucleation and glide. [8] Dislocation nucleation means that dislocations are created as atomic bonds along a line within the lattice break up. The consequence of the dislocation-formation is also called strain hardening, meaning that strengthening occurs due to the increasing dislocation-dislocation interaction and the correspondingly decreasing dislocation mobility. [9]
Cyclic strain hardening/softening: If it occurs due to cyclic loading, the strengthening of the material is called cyclic strain hardening/softening. The hardening/softening can be observed within the first cycles, as the maximum obtained stress increases/decreases with each cycle. Afterwards the material reaches a cyclically stable condition meaning that it does not harden/soften anymore.[10]

2.1.3 Dislocation Creep

Generally creep is the time-dependent form of irreversible deformation. If a load is applied to a material at an elevated temperature it causes strain to build up. [7]

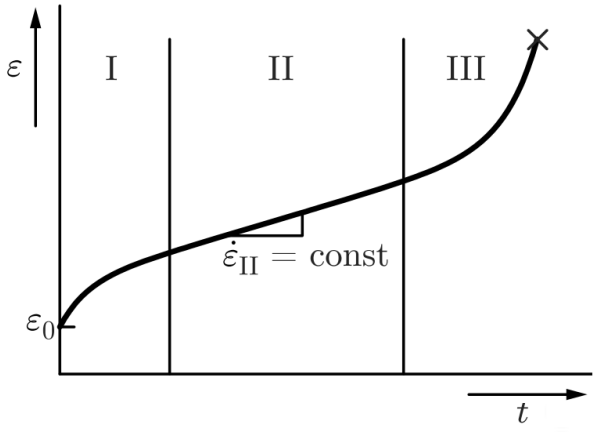

Figure 2: A diagram showing the evolution of strain (ϵ) vs. time (t) if a material is exposed to constant stress. [7]

The evolution of strain vs. time can be separated in three phases (see fig. 2): At the beginning of phase I (transient creep) the strain rate changes rapidly and lowers afterwards due to dislocation multiplication or rearrangement. In phase II (power-law creep), the strain rate stays nearly constant as the dislocation multiplication is in balance with dislocation annihilation. Phase III is the last phase as the material is damaged meaning that pores and/or small cracks arise. After a certain time, the material finally breaks (indicated with the cross in fig. 2). [7]
In copper, which is the material of interest in this thesis, power-law creep is the important

form of creep at higher temperatures. In this regime dislocations move through diffusion of vacancies or interstitial atoms. It is called power-law creep as the strain rate $\dot{\epsilon}$ is related to stress σ via a power law:

$$\dot{\epsilon} = c \cdot \left(\frac{\sigma}{\mu}\right)^n , \tag{1}$$

where c is a constant, amongst others depending on temperature and some diffusion constants, μ is the shear modulus and n is the so called creep-exponent. The diffusion constants change depending on whether high- or low-temperature creep (labelled as H.T.Creep and L.T.Creep in fig. 3) is apparent. The difference between these two regimes is that diffusion along dislocation cores is dominant at lower temperatures, whereas bulk diffusion is more prominent at higher temperatures. [11]

2.1.4 Diffusional Flow

At even higher temperatures, dislocation creep is accompanied by the so-called diffusional flow meaning that the diffusion of vacancies or interstitial atoms itself causes the deformation. Depending on the temperature the mechanisms differ from each other and therefore the diffusional flow regime can be subdivided into Nabarro-Herring creep and Coble creep.
Nabarro-Herring creep: The diffusion path goes through the interior of the grain, not along its boundary. The strain rate thus depends on the bulk diffusion constants.
Coble creep: In this case the vacancies do not diffuse through the grain but instead follow the grain boundaries. The strain rate depends on the grain-boundary diffusion coefficient. As the activation energy for diffusion along the grain boundaries is lower, this mechanism occurs at lower temperatures compared to the Nabarro-Herring-Creep.

In both cases grain boundaries instead of dislocations serve as sources and sinks for vacancies and the strain rate is proportional to the stress applied. The vacancies diffuse from the grain boundaries, which are orthogonal to the tensile stress to the boundaries at which the compressive stress is orthogonal. This means that the grain involved changes its shape meaning that also the surrounding grains have to follow. Thus, grain boundaries have to slide. [7, 11]

2.1.5 Deformation Mechanism Maps

Partially it was already mentioned that some of the deformation mechanisms are dominant at certain temperatures due to the needed activation energy. But of course all of the deformation mechanisms can be observed only in certain temperature regimes. In literature they are often related to the homologous temperature, which is the fraction of the temperature to the melting temperature of the material. Also the stress is often rescaled by dividing the shear stress by the shear modulus.
In a so-called "deformation mechanism map" the different deformation mechanisms are plotted for the regimes in the homologous temperature and normalized stress, at which they dominate. Figure 3 shows such a deformation mechanism map for copper. Note

that this map is valid for copper with a grain size of $d = 0.1\,\text{mm}$; for other grain sizes the map looks different as deformation depends on the microstructure of the material.

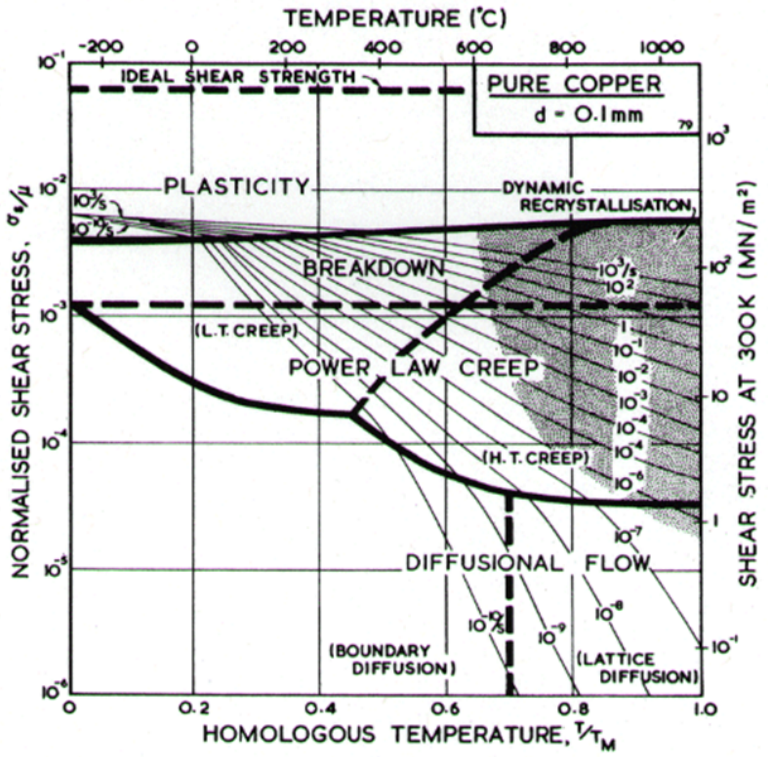

Figure 3: Deformation mechanism map for pure copper. [12]

2.1.6 Stoney Equation

If a stress develops in a thin film, which is attached to a substrate, film stress σ_f and substrate curvature c (measured in m^{-1}) are related to each other via Stoney's equation:

$$\sigma_f = \frac{E_S h_S^2}{6 h_f \left(1 - \nu_S\right)} \cdot c. \tag{2}$$

In this context, h_S is the thickness of the substrate, h_f the thickness of the film, E_S is the elastic modulus and ν_S is Poisson‘s ratio of the substrate. [13]
But of course the equation has some limitations, which are listed below: [14]

- The substrate has to be elastically isotropic meaning that the elastic modulus and the Poisson's ratio have to be independent of its orientation
- The substrate has to be much thicker than the film ($h_f : h_s \sim 1 : 100$) ensuring a purely elastic deformation of the substrate
- The film has to be a full film meaning that the substrate has to be completely and uniformly covered

- The temperature distribution within the whole stack has to be homogeneous

In semiconductor industry Stoney's equation is often used to obtain information about the stress in a certain film by depositing the material on a flat Si substrate and measuring the curvature. But as silicon is elastically anisotropic, the original Stoney equation has to be modified. [14]

2.2 Wafer Curvature based Stress Measurements in Thin Films

In this chapter the three experimental techniques, namely the wafer curvature system, the adapted wafer curvature system and the laser scanning Doppler vibrometer, are presented in more detail. Each of them has its special characteristics concerning sample size, measurement technique and heating/cooling rates.

2.2.1 Wafer Curvature Systems

Wafer curvature is a technique, where the bow of a sample (typically a wafer or a wafer piece) is monitored while being thermally cycled. Figure 4 shows a simplified schematics of a *k-Space* wafer curvature system that is available at *KAI*. [15] It includes a so-called *multi-beam optical sensor*, which allows curvature measurements based on the reflection of an originally parallel array of laser beams hitting the curved sample surface.

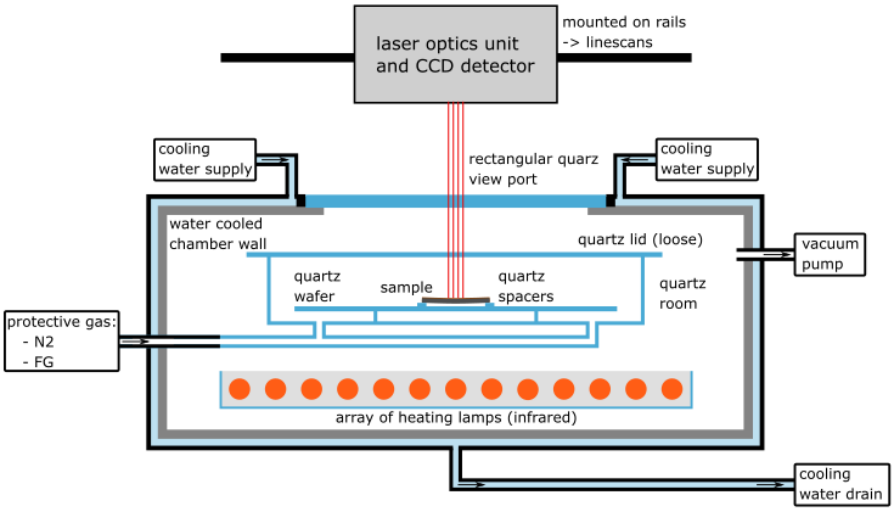

Figure 4: Schematics of a wafer curvature setup.

The sample is located in a chamber, which is heated via infrared lamps positioned at the bottom and can be cooled by a cooling water system integrated into the chamber walls. A thermocouple is used to monitor the temperature, which itself is used to control the heating/cooling system. Due to the large sample size and correspondingly large thermal mass of the chamber only comparatively low heating rates in the order of $0.2\,\mathrm{K\,s^{-1}}$ are possible. As water is used for cooling, no constant cooling rates can be met.

As illustrated in fig. 5, the curvature measurement is facilitated by the laser optics unit, which creates a laser array of several parallel beams that are directed onto the sample. Depending on the curvature of the sample, the beams are reflected at defined angles corresponding to a characteristic spot spacing of the beams at the CCD camera.
This means that the curvature of the sample can be calculated by measuring the distances between the spots on the sensor. Compared to a flat reference the relative distance of the beams hitting a curved sample is higher if the sample is convex and lower if the sample is concave.
The sample size must exceed the dimensions of the laser array, which is around 5.0 mm × 3.3 mm for the k-Space wafer curvature tool.

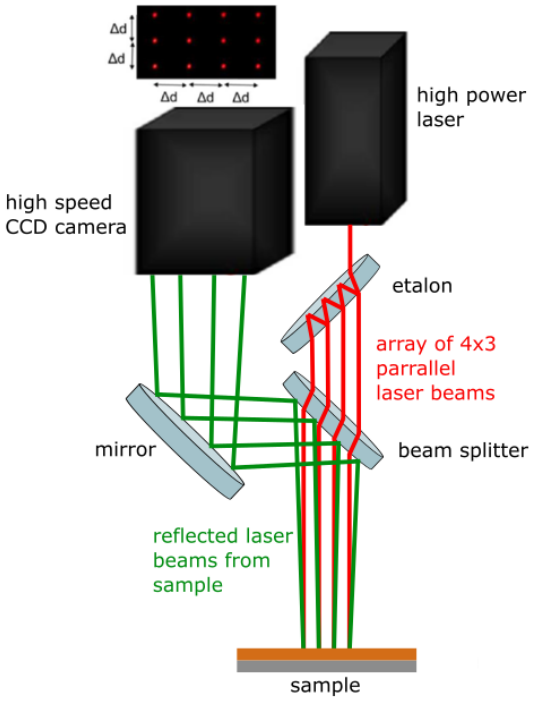

Figure 5: Illustration of the principle function of the k-Space system used for curvature measurements.

Figure 6 shows two representative curvature measurements performed on the k-Space system. The curves correspond to a wafer piece (20 µm Cu on 775 µm Si, size 4 cm×1 cm), which was subjected to thermal cycles with heating rates of 0.1 K s^{-1} and maximum temperatures of 320 °C and 420 °C, respectively.
Both measurements start at room temperature with the wafer piece being in a tensile stress state. The plot has to be read counter clockwise meaning that there is a linear-elastic behaviour during heating until a temperature of roughly 120 °C is reached. Afterwards the deformation mechanism changes into plastic deformation until reaching the maximum curvature in compressive state at roughly 220 °C. During further heating relaxation mechanisms become more and more dominating as the measured curvature

is approaching $0\,\mathrm{m}^{-1}$. But as the system starts to cool down, the curvature goes back to its original value again leaving the sample in a tensile stress.

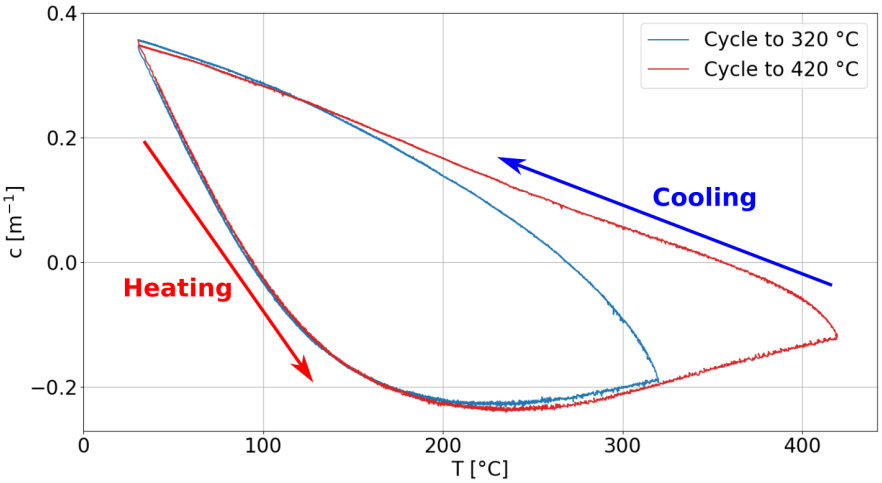

Figure 6: Two curvature-temperature measurements performed with the k-Space tool on a wafer piece (20 µm Cu on 775 µm Si) with a heating rate of $0.1\,\mathrm{K\,s}^{-1}$.
T: Temperature in °C; c: Curvature in m^{-1}

2.2.2 Adapted Wafer Curvature Systems

The biggest disadvantage of wafer curvature systems is their relatively low heating rate during the measurements. So-called adapted wafer curvature systems have higher heating rates, provide active cooling and allow measurements on smaller samples. As an example of an adapted system, the *thermal modified CT100 (tmCT100)* is presented, which was designed by *T. Heidmann* and described in detail in his master thesis. [16] It is a setup allowing the determination of temperature-dependent bow of small multilayer systems, e.g. wafer pieces. Compared to the conventional wafer curvature system its heating rates are higher (approximately $4\,\mathrm{K\,s}^{-1}$) but nevertheless it is still based on passive heating via a heating plate.

As illustrated in fig. 7, the sample lies on a stage with dimensions $35\,\mathrm{mm} \times 35\,\mathrm{mm}$. The stage is provided with both, a thermoelectrical heating system as well as a cooling system based on water and liquid nitrogen cooling. This allows maintaining predefined heating/cooling rates over a wide span in temperatures. In addition, it is possible to purge the temperature chamber with gas (e.g., nitrogen).

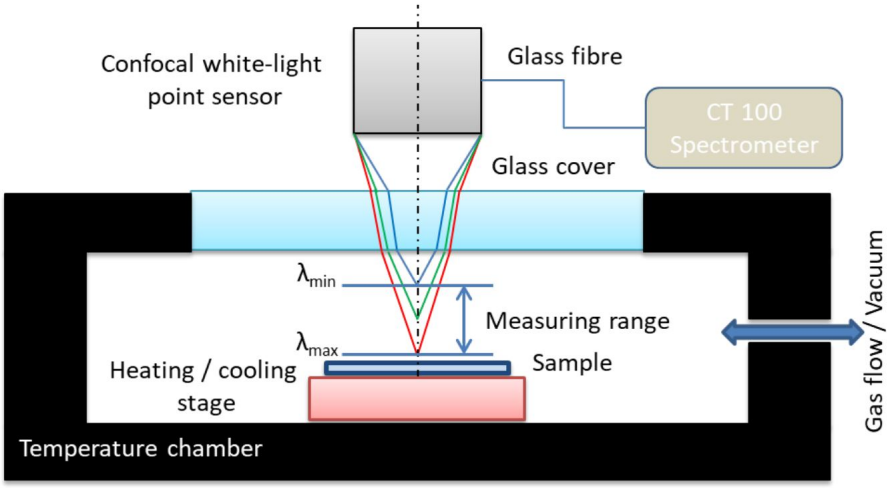

Figure 7: Schematics showing the tmCT100 measurement setup. [16]

The curvature measurement of the *tmCT100* is performed using white light interferometry, which is described in the following and illustrated in fig. 8.

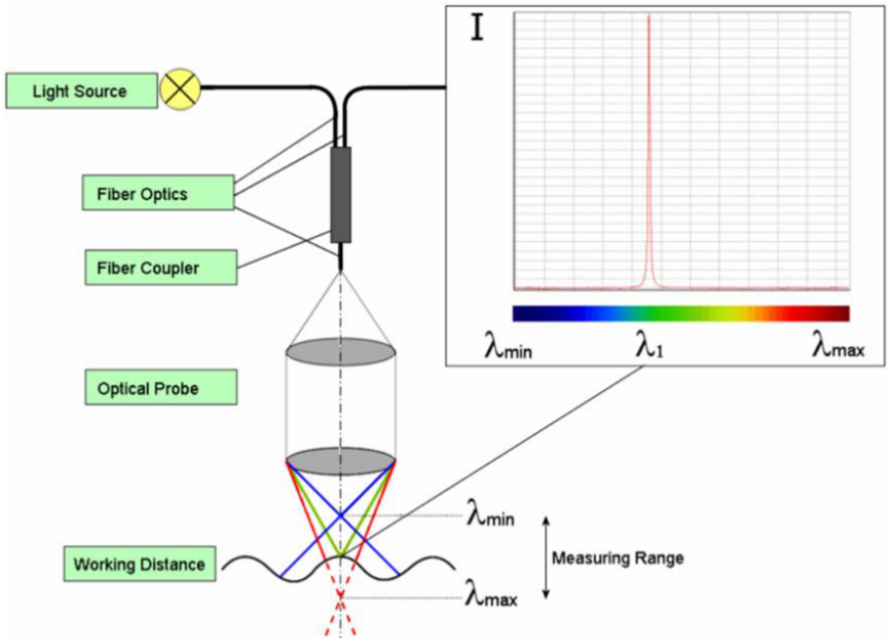

Figure 8: Working principle of a white-light interferometer. [16]

The white-light sensor includes a white light source, whose light is emitted onto the sample and the optical probe. Due to chromatic aberration the optical probe causes the white light to split into various colors, which are focused onto individual focal planes.

The analysis of the reflected spectrum using the spectrometer will thus result in a high-intensity peak at a certain wavelength, out of which the distance between optical probe and sample can be determined. As during a scan the stage is moved in x- and y-direction, the topography of the sample is obtained. The analysis of this data leads to the curvature of the sample.
To summarize the characteristics and limitations of the setup, the *tmCT100* can be used to measure pretty small samples (approximately 1 mm) with heating rates up to roughly $4\,\mathrm{K\,s^{-1}}$. The highest reachable temperature is 596 °C. [16]

2.2.3 Laser Scanning Doppler Vibrometry (LSDV)

A laser scanning Doppler vibrometer works based on the Doppler effect and can be used to either measure the eigenfrequencies of a sample or the velocity of a moving surface. The main advantage is that measurements on several points of the objects surface can be performed with a high temporal resolution.
For obtaining the curvature, the velocities of five points are integrated to obtain their displacements and a fit is performed for every time step (see sec. 3.4).

Doppler effect:
The Doppler effect can occur for all kind of waves such as, for example, sound or light. As light waves are the only important wave form in this work, the following paragraph focuses on them. A light source, e.g. a laser, emits light with a defined constant frequency. If the emitted light waves hit a moving object the reflected beam has a different frequency. The moving object this thesis focuses on is the surface of a polyheater during a temperature cycle.

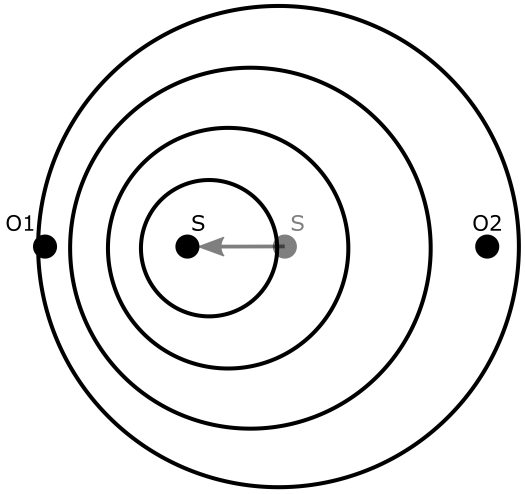

Figure 9: Schematics illustrating the Doppler effect
O1 and O2 are two stationary observers detecting the light emitted by the moving light source S. As the source is moving towards O1, he will observe an increased frequency, whereas O2 will observe a decreased frequency as S moves away.

The relation of emitted and reflected beam can be described via

$$f_O = \frac{f_i}{1 - \frac{v}{c}}, \tag{3}$$

where f_O is the frequency perceived by the observer, f_i is the frequency of the incident beam (in our case emitted by the laser), v is the velocity of the moving object and c is the speed of light. [17] As shown in fig. 9, the frequency can either increase or decrease depending on the position of the observer. If the source moves towards an observer, the wave maxima are compressed, which means that the frequency increases. On the other hand an observer from whom the source moves away will perceive a beam with a decreased frequency.

Vibrometer:
Laser scanning Doppler vibrometers are widely used for measuring velocities and displacements, respectively, of all kinds of samples. Their resolution ranges down to femtometer no matter how near/far the sample is. Another advantage is that the measurements are performed with light meaning that it is a non-destructive but also a very fast measurement technique. But there are also disadvantages: One of the most crucial ones is that vibrations of the environment have a huge impact on the measurement. Another one is that the laser beam is always focused on only one point. [18]

Principle function:
Figure 10 illustrates the basic setup and the principle function of an LSDV.

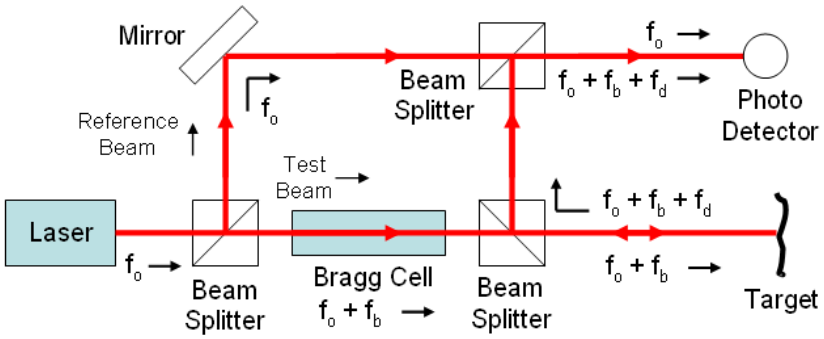

Figure 10: Schematic structure of an LSDV. [19]

A laser emits a light beam of a certain frequency f_0. This beam is split into a reference beam and a test beam at the first beam splitter. By following the path of the reference beam one can see that it is directed straight to a second beam splitter. The test beam on the other hand has to travel through a Bragg cell, which is used to shift the lights frequency by a frequency f_b. This is necessary for distinguishing the direction of the sample's surface movement as f_b increases in case the sample moves towards the detector

and decreases in case it moves away. After passing the next beam splitter, the laser beam hits the target. If the latter is moving, the frequency of the laser beam changes according to eq. 3. The beam is reflected by the sample and guided towards the upper beam splitter, where it combines with the reference beam. The merged beam travels to the photo detector, where it creates an interference pattern. [18]
The velocity of the target in direction of the laser beam is calculated using eq. 3, if the "observer frequency" (which in fig. 10 is the sum of f_0, f_b and f_d) as well as the incident frequency f_i are known.

3 Experimental Methodology

3.1 Device under Test (DUT)

The devices under test were so-called "polyheaters". These are special chips, which were designed for chip-bow measurements at very high, application relevant heating rates, [3] but also for several other experiments. [4, 20, 21, 22, 23, 24, 25] Within this master thesis polyheaters were used for curvature measurements during a short temperature pulse.

3.1.1 Structure of Polyheaters

Their structure resembles power semiconductors but some parts are replaced/changed to simplify testing. Figure 11 shows a schematic of a polyheater in cross-section. There are four layers needed for its functionality, which are explained in the following. The layers are separated by oxide layers for electrical insulation.

1. A silicon substrate with a nominally fabricated thickness of $h_{Si} = 120\,\mu m$. Silicon is the standard base material for most industrially fabricated semiconductor chips and for this reason also the polyheaters investigated within this thesis are based on silicon substrates. The purpose of the substrates is to provide mechanical stability during thermo-mechanical loading.

2. A highly phosphorus-doped polycrystalline silicon (polysilicon) layer with a thickness of $h_P = 300\,nm$. Due to doping its resistance can change but using the formula for a typical sheet resistance, its resistivity is approximately $R_{Sheet} = 20\,\Omega$ at room temperature. When an electric current flows through this resistive layer, it is heated due to Joule heating. The produced heat H is related to the applied current $I(t)$ via
$$H = \int_0^{t_{pulse}} I(t)^2 \cdot R_{Sheet}(t) dt \tag{4}$$
where t_{pulse} is the duration of a pulse. The resistance of the polysilicon changes with time as the polysilicon is heated.
The heating power can easily reach several Watts causing a fast temperature rise of several Kelvin per millisecond. It does not only cause the polysilicon to heat up but also spreads over the surrounding materials.

3. A small aluminum line, which is used as temperature sensor based on a 4-point resistance measurement. As the resistance of the temperature sensor lies in the Ω-range, the measurement error has to be very low. In general a resistance measured using the 4-wire method does not include the resistance of the connections lines, which in case of the 2-wire method would be added resulting in incorrect values. The 4-wire method is based on a current force and a voltage sense circuit. The first provides a stable DC current, which is forced through the temperature sensor resistance; the latter is used to measure the corresponding voltage drop across

it. The advantage is the negligible error in the voltage measured as the input resistance of the voltmeter is very high.
The resistance of the aluminum line is then obtained via Ohm's law using the pre-defined force current and the voltage drop measured. It is related to the temperature according to

$$R(T) = R(T_0) \cdot (1 + \alpha\,(T - T_0)) \tag{5}$$

where $R(T)$ is the resistance measured in dependence of the temperature, $R(T_0)$ is the resistance measured at the known temperature $T_0 = 20\,°\mathrm{C}$, α is the temperature coefficient of aluminum and T is the temperature. The temperature coefficient with respect to $T_0 = 20\,°\mathrm{C}$ was determined to a value of $\alpha = 0.003\,72\,\mathrm{K}^{-1}$. The experimental setup used within this thesis allows measuring the temperature profile during a heat pulse with a high temporal resolution. For this purpose, the concept of 4-wire resistance measurement is employed. The voltage drop is measured using an oscilloscope, while a 5 mA current is forced through the temperature sensor resistance.

4. The topmost 20 µm thick copper metallization, which is investigated in this work. As after the silicon substrate it is the second thickest layer in the stack, these two materials are the most contributing ones in terms of bow of the polyheater during a temperature pulse. The bow during increasing temperature is caused as the layers have different CTEs. Previously aluminum was used instead of copper but it was replaced as copper has better thermal and electrical properties resulting in a slower thermo-mechanical fatigue. [26]

Figure 11: Schematic cross-section of a polyheater (not to scale).

3.1.2 Layout

An optical microscopy image of a polyheater as a whole is shown in fig. 12. It has a size of roughly $2\,\text{mm} \times 3\,\text{mm}$ and the square shaped copper plate in the center (circled in green) is the part, which is investigated during the thermo-mechanical chip bow experiments. The outer copper pads are used to electrically contact the polyheater. The big ones labelled as "Polysilicon" are the contacts to the polysilicon layer, to which the power pulses are applied as well as at which the voltage drop and the current are measured. It is important to mention that the polysilicon has roughly the size of the central copper plate meaning that only the central part of the polyheater is actively heated during a power pulse.

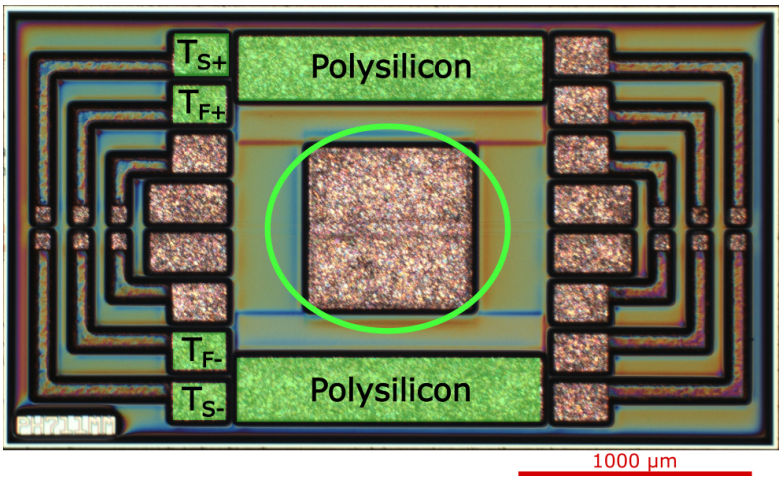

Figure 12: Top view of a plate polyheater recorded using a light microscope.

As labelled in fig. 12, the outer four of the smaller pads on the left side correspond to the temperature sensor that was used for the measurements described in this thesis. The force circuit of the 4-wire measurement explained in sec. 3.1.1 is connected via T_{F-} and T_{F+} and T_{S-} and T_{S+} are for sensing the voltage.
There is a second temperature sensor (not labelled) on the right side of the chip to make the polyheater completely symmetrical. However, it was not used during any of the measurements.

3.1.3 Thinning

As the curvature scales with the square of the substrate thickness (see eq. 2), the DUT was thinned to increase the signal measured. For the thinning, an *Allied X-prep Precision Milling/Polishing System* at *Infineon Villach* was used. Since the thinning procedure was used the first time for polyheater samples in this work, it is desribed in detail in the following using the information given in the brochure of the system mentioned. [27]
The X-Prep is a Computerized-Numerical-Control-based machine, which can be used for milling, polishing and grinding. Samples can be thinned with high precision, i.e.,

1 µm accuracy for the z-axis. Despite the spindle it also includes a camera, which allows sample imaging. The process can be divided in five steps, which are:

1. **Mounting:** The mounting is performed by gluing the sample onto a glass carrier in order to ensure that it does not slip away during the milling and polishing steps. Within this procedure a glass carrier is put on a heating plate heated up to a temperature of 150 °C to allow the melting of a wax. To prevent the sample from breaking during the following milling and polishing processes, one has to ensure that it is completely underlaid by the wax. Afterwards the glass carrier is taken off the heating plate and one has to wait some minutes until the wax is solidified. The glass carrier with the sample attached on it can now be put into a special fixture of the X-prep, which is fixed on the holder.

2. **Levelling:** For a uniform material removal, each sample has to be aligned in parallel with the horizontal plane, in which the tool moves. After inserting the special levelling tool a dual-axis tilt control is performed. The correction is repeated until the sample is levelled up to a tolerance value set by the user. During operation, the tolerance was set to its minimum value of 0.5 µm, which means that the distance between all edges of the sample and the tool is accurate to 0.5 µm.

3. **Milling:** For the milling one has to consider that the metal bond diamond tool has to move over the edges of the sample to ensure a complete material removal. The exact position depends on the size of the tool as it should be around half of its diameter. Afterwards the desired amount of material to be removed as well as the rotating speed, the feed rate and the overlap (set to 75 %) of the tool have to be entered and the "Position mode" has to be enabled. The latter means that the tool is kept at a constant height during milling by changing the force applied. Before starting the milling process, it is important to fill the stage with a solvent-free lubricant to ensure cooler cutting temperatures for avoiding overheating of the sample as well as minimizing tool wear.

4. **Polishing:** For every polishing step, first a new polishing attachment has to be put on the polishing tool. Therefore a small disc with the size of the polishing tool (in our case 1.5 mm) has to be glued onto the socket. A diamond compound is applied onto the sample together with a drop of the lubricant mentioned above. The compound consists of small polycrystalline diamonds with a size of either 30 µm, 9 µm, 3 µm or 1 µm. For each step only one of them can be used. The selection depends on the desired final surface roughness. Again the same parameters as during milling have to be set. There are only two differences: The overlap has to be set to 85 % (for 30 µm and 9 µm polishing paste) or 95 % (for 3 µm and 1 µm polishing paste) and the mode has to be changed to "Position Force mode" meaning that the tool presses on the sample with a constant force. For polyheater samples only the 30 µm and 9 µm polishing pastes were used so the force was set to 1.2 N.

5. **Dismantling:** At the end the glass carrier is taken out of the fixture. It is put in an acetone bath for dissolving the wax, which takes several hours. Finally the individual samples can be taken out.

After the thinning process is completed, the substrate thickness of the sample is measured with an infrared interferometer. As an example, the results of a sample which was thinned to a silicon thickness of 60 µm are shown in fig. 13. The microscope image (fig. 13a) shows that the surface is not perfect as it includes some bumps, which arised during the thinning step and could not be polished away completely. This occurred for every sample thinned but as the steps are not unique, also the surface of each sample is individual. Also the interferometer measurement (fig. 13b) shows that the surface is a little bit rough. Nevertheless the whole thinning processes for all the samples used in this thesis met the substrate thickness desired very well and is reproducible within roughly 3 µm.

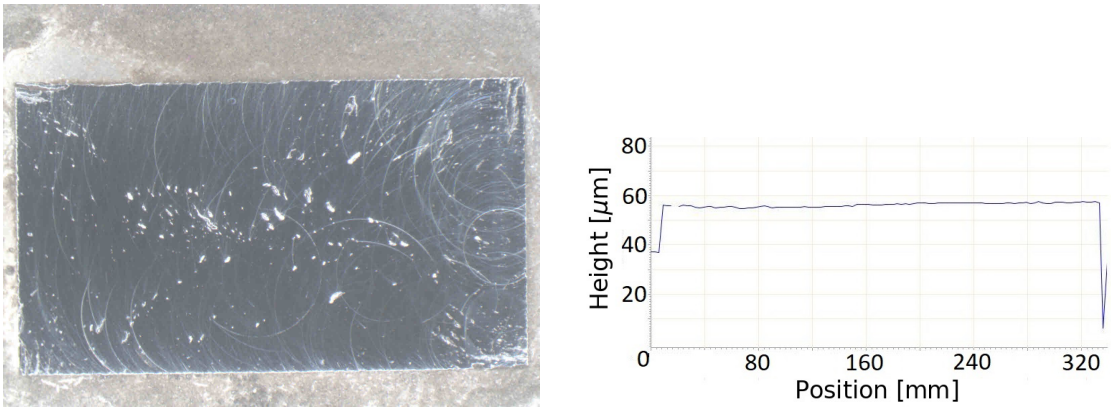

(a) Bottom view image of a sample

(b) Result of the interferometer measurement

Figure 13: Example sample after the whole thinning process.

3.2 Measurement Setup

In this subchapter the whole measurement setup including the probecard, the setup for pulsing the DUT, the programmable current source providing arbitrarily programmable current pulses and finally the LSDV for the velocity measurements are presented and explained.

3.2.1 Probecard

A probecard is a special mechanical construction that allows electrically contacting the individual pads of a chip using contacting needles. Instead of using wire bonded and packaged devices, the usage of a probecard allows working with bare chips. As for the curvature measurements presented in this thesis the polyheaters are required to have an exposed metallization surface the usage of packaged devices would anyhow not be possible. In addition packaged samples are glued to a leadframe, which decreases the

bending drastically. The basic components of the probecard used within this thesis are listed in the following:

- A carbon alignment plate used to place the polyheaters precisely
- A moveable lid including several contacting needles, which can be opened for changing the sample
- A screw to fix the moveable lid to the ground plate
- A cable to connect the probecard to the polyheater setup

If the moveable lid is opened, the probecard looks as shown in fig. 14. One can see the carbon alignment plate, allowing to precisely position a polyheater on the probecard such that its pads can be contacted by the needles when closing the lid. It also ensures that the sample stays in place during the measurement. As briefly mentioned in sec. 3.1.2 and shown in fig. 12 the polysilicon pads are much bigger than the ones used for measurements. The reason for this is that high currents have to be applied to the polysilicon (peak values above 2 A are possible). By distributing the current over multiple needles the current in the individual needles can be reduced. As for the 4-wire resistance measurements of the temperature sensor only low force currents are used (as mentioned in sec. 3.1.1) it is sufficient to contact the respective pads by just one needle each.

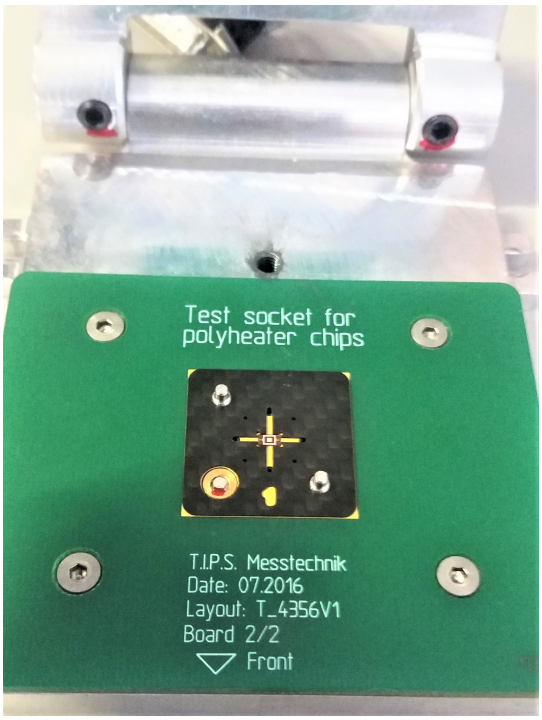

Figure 14: The exposed probecard showing the carbon alignment plate (black) with the polyheater placed in its center.

3.2.2 Polyheater Setup

S. Moser, G. Zernatto et al. described the original version of the polyheater setup, which allows stressing polyheaters in situ while monitoring their degradation by means of scanning electron microscope imaging and electrical measurements in their paper. [3] This chapter explains the setup as well as the upgrades that were implemented within this thesis: the installation of both a programmable current source and the laser scanning Doppler vibrometer, which are necessary for performing the chip bow experiments.

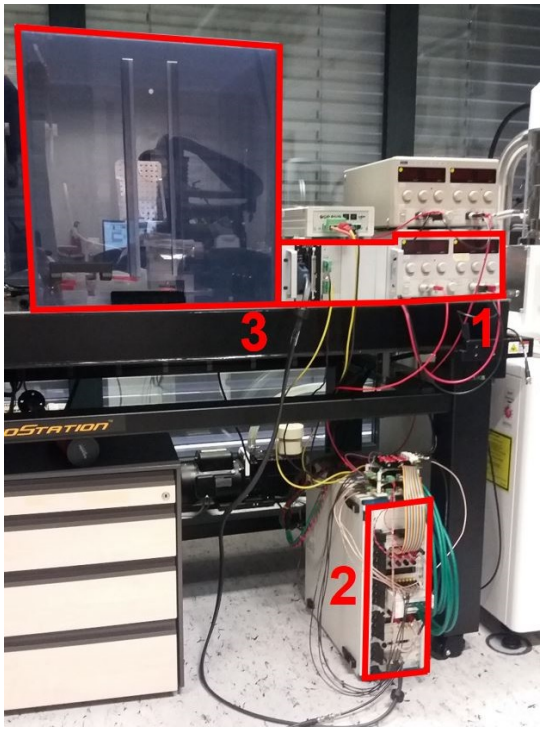

Figure 15: A photograph of the setup used for pulsing the samples. The different components are: programmable current source (1), PXI chassis (2) and HV box (3).
e.

Figure 15 shows the already modified setup designed to provide heating pulses to study the thermo-mechanical behaviour of polyheater devices at high heating rates. As highlighted in fig. 15, the components of the experimental setup are:

1. A programmable current source (described in more detail in sec. 3.2.3) together with the power supply

2. A PXI chassis, which contains several technical instruments comprising a digital multimeter used for electrical resistance measurements, an I/O module for generating pulses and a digital oscilloscope for characterising the pulses

3. A high voltage box (HV box) where the needle card is placed inside to avoid

measurements being affected by the environment, e.g. by the air condition in the lab

Figure 15 also shows the vibration isolation table, on which the whole setup and also the scanning head of the vibrometer are mounted to minimize environmental vibrations.

As can be seen in fig. 16, one wall of the HV box has a hole, through which the scanning head of the LSDV can be put. This allows the laser to directly hit the sample. The probecard is mounted on a special holder, which allows movements both in horizontal and vertical directions in order to precisely align the needle card with respect to the LSDV. At the top of the needle card the cable from the polyheater setup can be plugged in.

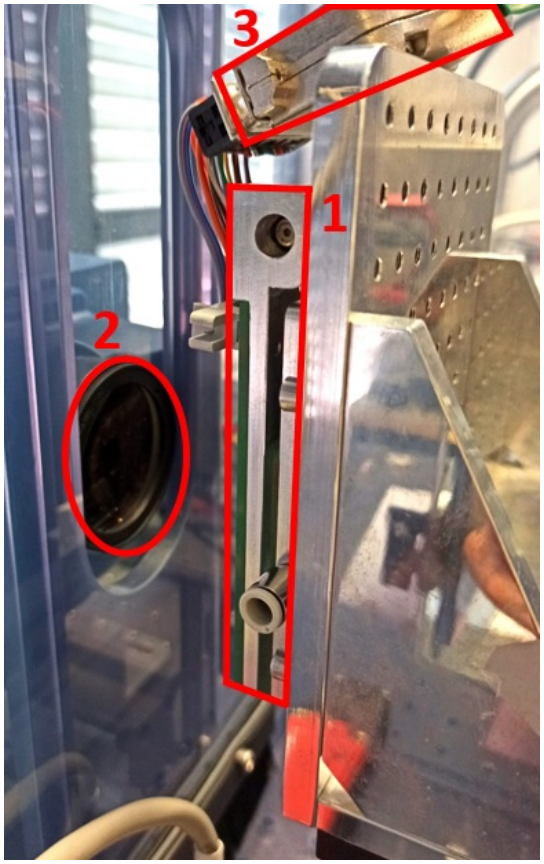

Figure 16: A photograph showing the inside of the HV box. The probecard (1) is mounted on a holder and placed in front of the front lens (2) of the scanning head of the vibrometer. On top of the picture the cable (3), via which the probecard (and its inserted polyheater) is connected with the polyheater setup, can be seen.

3.2.3 Programmable current source

The specially designed programmable current source (ARCTIS system) integrated to the polyheater setup is designed for repetitively stressing a DUT using piecewise linear current pulses.
The desired current profile during a pulse is defined by a vector of up to 16 data pairs consisting of a time and an associated current coordinate. When reproducing one such predefined current pulse the individual data pairs are interpolated by straight connection lines resulting in a piecewise linear (PWL) current profile. Considering the resolution of the system, this basically allows arbitrary shaping of current pulses, which are then applied to the DUT. One disadvantage of the setup by *Moser and Zernatto* [3] is that it is only capable of providing rectangular shaped voltage pulses with a non-linear heating characteristics. The adaption of the system towards the programmable current source was a necessary step to achieve linear heating and cooling rates during pulses.
In general, when defining an arbitrary pulse using the ARCTIS setup it is important to keep four points unchanged. At the beginning of every pulse, two points with a current value of 50 mA are necessary to "pre-charge" the controller of the I-driver. At the end of every pulse, two points with a current value of 0 A are needed as the last point of the pulse is kept until the device is shut down. During the experiments the step at the beginning was not only used for pre-charging but also for triggering the LSDV (see sec. 3.3.2).

3.2.4 LSDV setup

The basics of the LSDV were already explained in sec. 2.2.3. As mentioned, the LSDV is from *Polytec*. Its main parts arei. explained in the following and shown in fig. 17:

- **Scanning head PSV-400:** It is the most important part of the setup as it comprises all the components shown in fig. 10. The included helium-neon laser is characterized by a wavelength of 633 nm and the Bragg cell has a modulation frequency of 40 MHz. Besides the optical components, the scanning head is additionally equipped with a video camera, which provides a video image of the samples surface. [28]

- **Junction box:** It is used to connect all the other components and includes the inputs (e.g., for a reference signal), the outputs of the internal frequency generator as well as digital inputs and outputs, which are, e.g., used for the external trigger.

- **Vibrometer controller OFV-5000:** The signal of the scanning head is decoded by one of the two available velocity decoders *VD-07* or *VD-09*. This is done by creating an analogue voltage signal proportional to the velocity of the samples surface.

- **Data management system:** This is a PC, which provides the software for controlling the LSDV as well as collecting and saving the measurement data obtained. It also includes an analysis tool for post-processing the raw data.

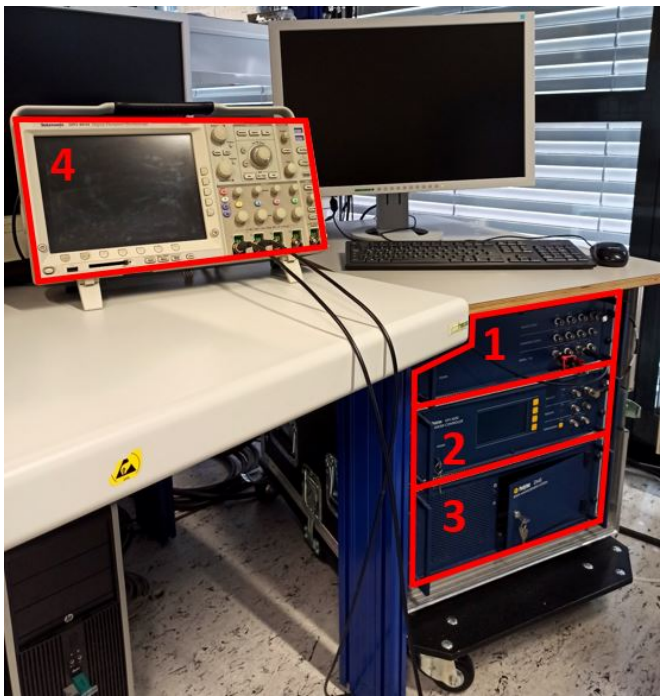

Figure 17: The different components of the LSDV setup. The junction box (1), vibrometer controller (2) and data management system (3) together with the external oscilloscope (4). Although the scanning head is not on the picture, it is the fourth important part of the LSDV setup.

3.3 Measurement Procedure

The goal of each measurement is to obtain the raw data, which is used to calculate the curvature-vs-temeprature curves. Therefore several steps have to be performed including the definition of the current profile to reach the desired maximum temperature with a constant heating rate. Also the settings for the LSDV have to be set to ensure optimal measurement conditions as well as to define the points at which the LSDV measurements are performed. As a separate pulse for each point is needed, the reproducibility of both, the current pulse as well as the vibrometer measurement, is important. As the material changes within the first few pulses (see sec. 4.2.2), the curvature measurements are started after 10 pulses are performed.

3.3.1 Preparations

At first the LSDV is turned on as it takes about 30 minutes to heat up the He-Ne laser. During this time the remaining steps described in this section can be done.
The sample, which needs to be tested is put into the probecard. For thinned chips, an additional "spacer" has to be used to achieve the required height that is needed for the needles to contact the pads of the polyheater well. The spacer simply is a polyheater

thinned to 60 µm as the samples used for the measurements presented in this thesis are thinned to a substrate thickness of 60 µm and the probecard was initially designed for polyheaters with 120 µm thick substrates. After the thinning the copper pads of the spacer were etched to make sure that the spacer does not influence the curvature measurement.
After the polyheater is put in, the probecard can be mounted on the holder, which has to be placed in focus of the laser beam emitted from the scanning head. The connection to the polyheater setup should be checked by measuring the resistance of the temperature sensor at room temperature using the digital multimeter integrated in the PXI system. Finally, the HV box can be closed, the power supply unit can be turned on and the pump of the scanning electron microscope (a technical instrument that is loacated next to the polyheater setup but not required for the curvature experiments) has to be turned off to reduce environmental vibrations (see sec. 4.1.4).

3.3.2 Defining the Current Profile

If all devices (PXI, current source and the power supply) are switched on, the LabView program can be started and the parameters for the arbitrary pulse shape can be loaded.

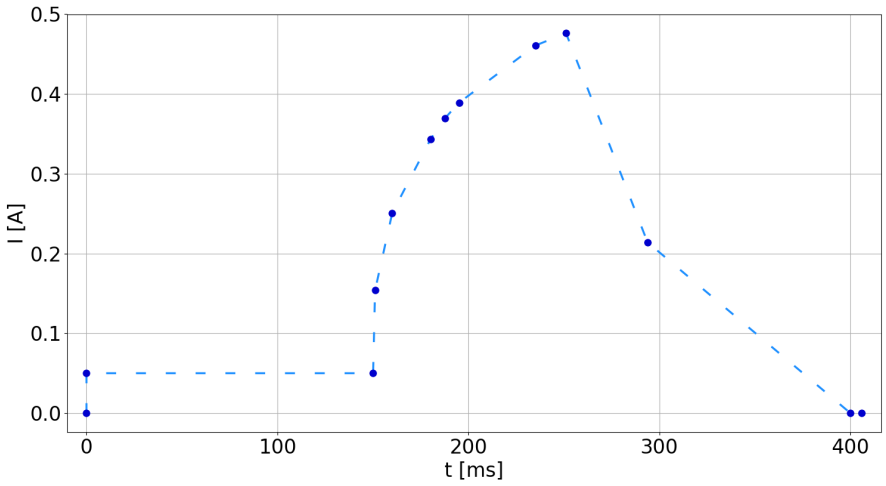

Figure 18: A current pulse given by 13 time/current pairs (darkblue). The dotted line represents the PWL signal.
t : Elapsed time in ms; I : Current in A

The pulse shape for heating a polyheater to 320 °C within 100 ms is shown in fig. 18. As mentioned in sec. 3.1.1, the heat produced is related to the integral of the current squared. This is why a current following a square root function results in an approximately constant heating rate and thus a linear temperature increase (the temperature profile corresponding to the current pulse plotted in fig. 18 is shown in fig. 19a). After reaching its maximum value the current is not immediately set to 0 A but instead follows empirically obtained time-current coordinates to enable linear cooling.

After loading the pulse parameters, either one single pulse - usually a test pulse to check the peak temperature - can be fired or the repetitive mode can be activated to periodically apply pulses until a manual stop. This mode was used for the curvature experiments, for which a wait time of 10 s between consecutive pulses was set.

3.3.3 LSDV settings

The menu of the LSDV shows several setting options. They are explained in the following and have to be individually set for each measurement as they define, under which parameters the measurements are performed. By this means, among other things also the highest measurable velocity as well as the duration of a measurement are defined.

General: In this part one can choose whether the measurement should be performed in frequency or time domain. Measurements in frequency domain lead to the frequency spectrum of the sample and can be, e.g., used to find the eigenfrequencies of a test device. On the other hand measurements in the time domain give the velocity of the samples surface vs. the measurement time. Polyheater measurements were thus always performed in time domain.

Channels: This tab shows a list of the channels, which are connected to the junction box. The only important one in our case is the vibrometer channel, for which one has to choose the input range. The lowest possible value is 200 mV, the highest one is 10 V. As a lower value results in a better quality of the measurement signal, polyheater measurements were performed with the lowest possible value (see sec. 4.1.2).

Filters: Here a high-, a low-, or a band-pass filter can be included resulting in certain blocked frequencies in the measurement. Also either velocity or displacement as data output can be chosen. During all polyheater measurements no filters were applied and the velocity was selected as output data.

Time: This option is only present if measurements are performed in the time domain. It allows choosing the sampling frequency in a range of 256 Hz to 2.56 MHz as well as the number of sampling points and shows the corresponding measurement time. The software allows at most 2^{26} measurement points but due to the size of the file created, measurements with more than 2^{19} points cannot be exported. The corresponding measurement time can be calculated via

$$t_{Meas} = \frac{number\ of\ samples}{sampling\ frequency}. \tag{6}$$

Trigger: The measurements can either be started manually or by means of a trigger signal (i.e., internal, external, or analogous trigger). As the vibrometer measurements had to be precisely synchronized with respect to the power pulse, the vibrometer was triggered externally using an oscilloscope (see fig. 17), which in turn triggered with the

rising edge of the voltage applied to the polysilicon layer of the DUT.

Vibrometer: Here the measurement range (in $\mathrm{mm\,s^{-1}\,V^{-1}}$) can be set. Together with the parameter chosen in the channel options, this determines the maximum measurable velocity v_{Max} according to

$$v_{Max} = mr \cdot V_{in}, \tag{7}$$

where mr is the chosen measurement range and V_{in} the input range for the channel.

Generator: If the generator is active, a sample can be excited with, e.g., a sinusoidal voltage signal by the internal generator of the setup. But as the polyheaters do not have to be excited, the generator was always switched off.

3.3.4 Performing the Measurement

After all the preparations are finished, multiple measurement points on the copper surface of the polyheater have to be chosen and saved to the software of the LSDV. In sequential order, at each of these points the vibrometer is going to perform a velocity measurement during a pulse. As already mentioned five measurement points were used for the experiments.
To make sure that the sample is in an equilibrium state and no "first cycle effects" occur (see fig. 31 in sec. 4.2.2), 10 pulses are applied before the actual measurement is started. To increase the signal to noise ratio of the data, the vibrometer measurements are repeated three times and the data of each point is averaged afterwards. After the three individual measurements are completed, the repetition mode of the programmable current source is aborted by stopping the LabView program of the programmable current source.
The velocity files can be exported in ASCII format using the analysis tool mentioned in sec. 3.2.4. This tool is also used to export the coordinates of the individual points. As the data for calculating the temperature is measured with the digital oscilloscope, its data is saved in a separate file.

3.4 Data Analysis

After finishing the measurement the obtained data of temperature vs. time as well as velocity vs. time has to be post processed to obtain the desired curvature-temperature relation of a sample. Therefore, an analysis program was written. The environment used to write the Python code was the *Scientific Python Development Environment (Spyder)*, which was released in October 2009 and initially developed by *Pierre Raybaut*.
The steps, which are performed with this program are shown in this sub chapter on the base of an experiment reaching a maximum temperature of about 320 °C in 100 ms. As input data the data analysis script requires the file containing the data for the temperature profile, the coordinate file of the measurement points on the polyheaters surface as well as the averaged velocity of each individual point. For the latter a second program calculating the average velocity of a point was written. It simply takes all the

velocities measured at a certain point, averages them over time and saves the averaged data in a separate file. This is done to reduce the noise during measurements as well as to adjust outliers. The averaged velocities are integrated afterwards to obtain the corresponding displacements.

3.4.1 Recalculation of Temperature

Due to the fact that the oscilloscope (temperature measurement) is not synchronized with the vibrometer (measurement of velocities) there is a shift in time for the corresponding measurement signals of one and the same pulse.

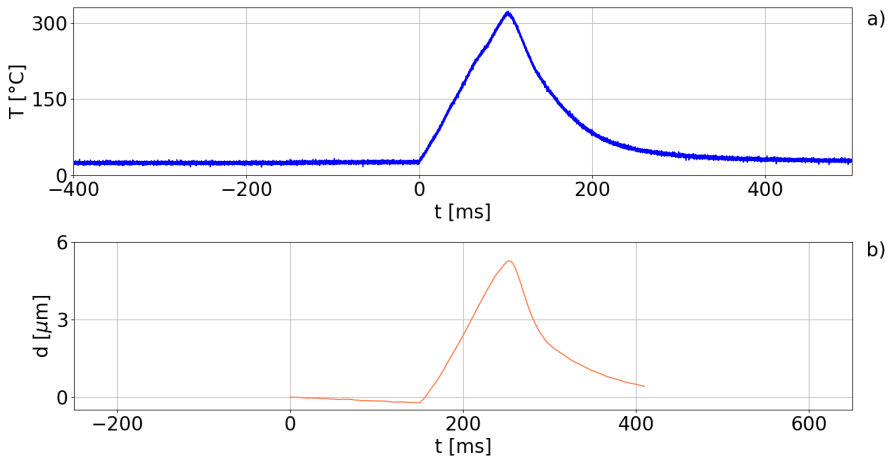

Figure 19: The temperature signal (a) and the displacement measured (b) of one power pulse indicating the different time scales and measuring times.
t: Elapsed time in ms; T: Measured temperature in °C; d: Measured displacement in µm

Figure 19 shows the measured temperature signal as well as the corresponding displacement measurement. As one can see, the vibrometer measurement starts 150 ms before the pulse whereas the zero point of the oscilloscopes time scale is at the starting time of the pulse. One part of data analysis thus is to "shift" the temperature to the time scale of the displacement. Therefore, at first the temperature file is read in. In the next step, the voltage drop over the temperature sensor has to be converted into temperature values as explained in sec. 3.1.1.

For changing the time scale the temperature vs. time is interpolated and recalculated such that it matches the time increment of the displacement measurement. Finally it is shifted by the desynchronization time (see fig. 20) such that it is synchronized with the vibrometer data, where the pulse starts at 150 ms.

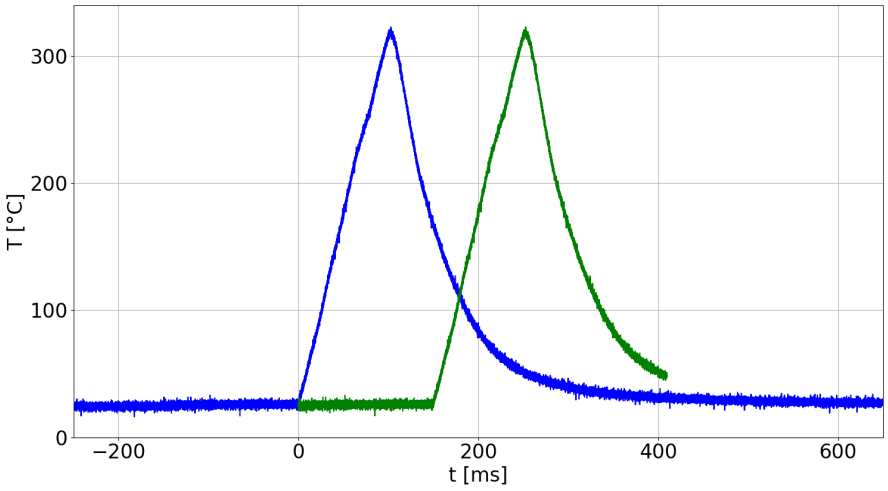

Figure 20: Original temperature signal (blue) and the correspondingly interpolated and shifted result (green).
t: Elapsed time in ms; T: Temperature in °C

3.4.2 Drift Correction

As mentioned the velocities are integrated to obtain the displacements of the sample at the different points. This is necessary as the curvature of the DUT later is calculated from a fit through the five displacement values.

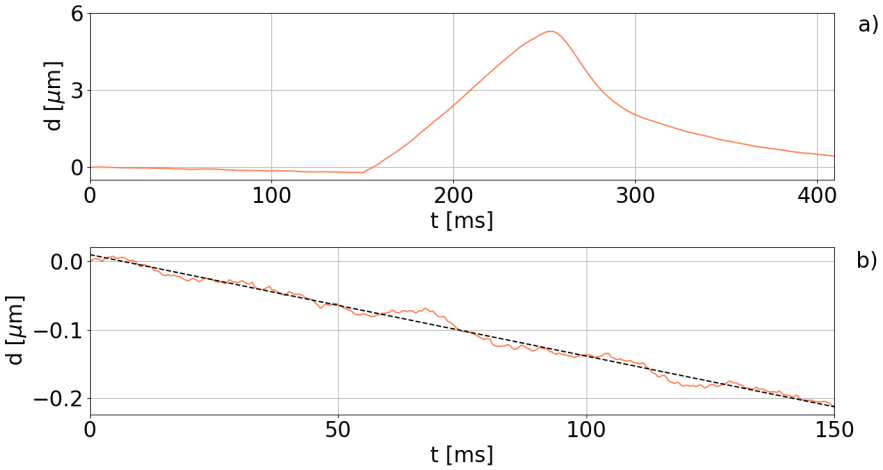

Figure 21: Measured displacement curve (orange) for a total measurement time of roughly 400 ms (a) as well as the linear fit (b) of the time before the pulse.
t: Elapsed time in ms; d: Measured displacement in µm

Figure 21a again shows the complete vibrometer measurement (note that starting with fig. 21 the time scale is adjusted to the measurement time of the vibrometer in all

following plots). In the time before the pulse (first 150 ms) no change in displacement should be observed, as the temperature stays constant and the sample is steady. In fig. 21b, which shows the first 150 ms of the displacement curve in more detail, it can be clearly seen that a displacement unequal to 0 µm is measured. In the context of this thesis this behaviour was referred to as drift. Figure 21b also shows the linear fit of the displacement, which is used to correct the drift for the whole pulse. The linear function was chosen as measurements on static polyheaters (not during a pulse) indicated that the drift has a linear characteristic.
In sec. 4.1 some settings for lowering the drift during measurements are presented. But even if they are applied a small drift remains, which has to be corrected.

3.4.3 Calculation of Curvature

The curvature cannot be measured directly with the vibrometer; instead, the displacements of five different points on the copper metallization (see fig. 22) are measured.

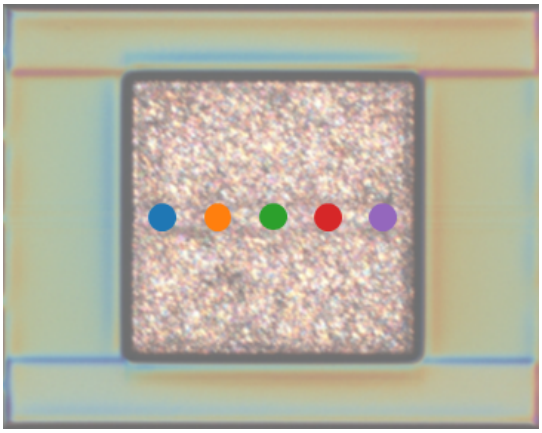

Figure 22: Top view of the central copper plate of a polyheater including the five points, at which the velocities/displacements are measured.
(Point 1 = blue, Point 2 = orange, Point 3 = green, Point 4 = red, Point 5 = violet)

As mentioned in sec. 2.1 and indicated in fig. 1, the copper surface of the polyheater will bend like a parabola during a tempereture increase, which is why five points were chosen to represent the global deformation of the copper plate. Theoretically, three measurement points would be sufficient to fit a prabola. The number of measurement points has to be a trade off between a high number of points as this increases the accuracy of the fit and a possibly low number as every additional point means that the polyheater has to be exposed to additional power cycles.
One measurement leads to the data presented in fig. 23. Note that the drift correction as well as the constraint that all five measurements start at $d = 0\,\mu m$ has already been applied, which would indicate that the surface of the polyheater is completely flat at the beginning of the measurement. In fact this is not true as the polyheater is already

slightly bend (to an unknown amount). The displacement is calculated by integrating the velocity, meaning that all five points start at $d = 0\,\mu m$, which means that the vibrometer can basically only be used for measuring changes in the displacement, not their absolute value. As those displacements are later used for calculating the curvature, also only changes in curvature can be measured, not the absolute curvatures.

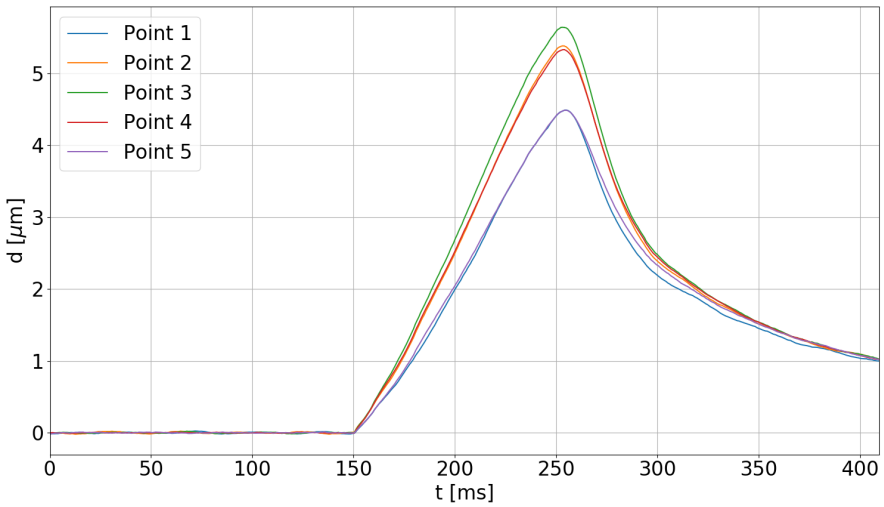

Figure 23: The measured displacements after the drift correction. As expected, the central point (Point 3, green) has the highest displacement.
t: Elapsed time in ms; d: Measured displacement in µm

For every time step one obtains five displacement values corresponding to the five measurement points on the polyheater. Now the analysis program has to perform a parabola fit for each time step resulting in the fit parameters a and b according to

$$d(r) = a \cdot r^2 + b \tag{8}$$

where $d(r)$ is the displacement depending on the position r of the measurement points on the copper plate of the polyheater. The latter is calculated via

$$r = \sqrt{x^2 + y^2} \tag{9}$$

where x and y are the position coordinates of the measurement on the polyheater obtained from the coordinate file mentioned in sec. 3.4, in which the central point (Point 3) is characterized by x- and y-coordinates of 0 µm each. This is the reason why the linear term is not included in eq. 8. The value r was chosen to be used instead of the x-coordinate to include the possibility that not all points lie on a horizontal axis. Although fig. 22 shows points, which all have the same y-coordinate this is not true for all the measurements.
If the sample is now heated and thus its curvature changes, the fit parameters a and b

will change. The curvature of the polyheater at a given time step t^* is now obtained via

$$c(t^*) = 2 \cdot a(t^*), \tag{10}$$

as the curvature generally is given by the second derivative of a function.
Figure 25 shows the displacement values of all of the five points together with the fit through them at seven time steps. Looking at the single diagrams already indicates the expected result, namely that the curvature increases during heating (fig. 25a, 25b and 25c) reaches its maximum at the maximum temperature (fig. 25d) and decreases back to a value of $0\,\mathrm{m}^{-1}$ during cooling (25e, 25f and 25g).
After the fits are performed for all time steps, the temporally resolved change in curvature during a pulse is obtained (see fig. 24).

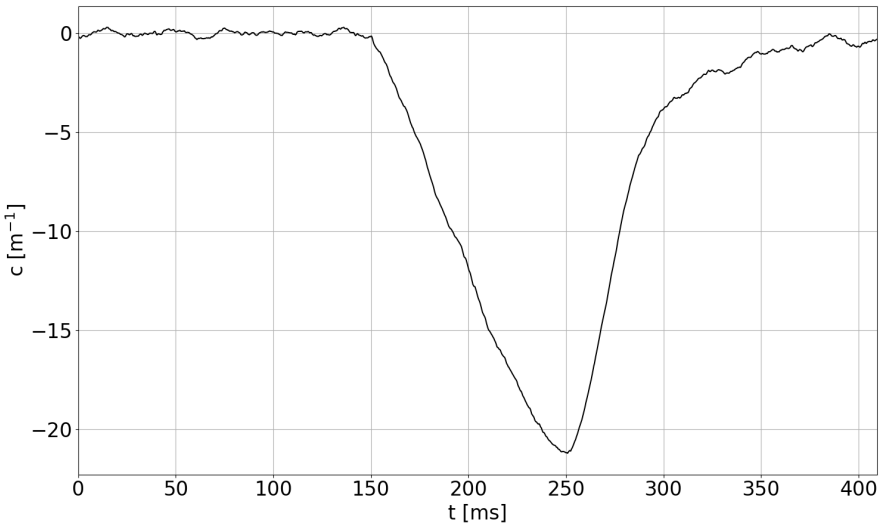

Figure 24: The curvature calculated out of the fits and plotted versus time.
t ... Elapsed time in ms; c ... Calculated curvature in m^{-1}

Again note that the curvature starts at $0\,\mathrm{m}^{-1}$ at the beginning of the measurement due to the constraints that have been included in the data processing script. As the curvature is calculated out of the displacements and all the displacements start at $0\,\mu\mathrm{m}$ (see fig. 23), no information about the initial curvature can be obtained out of the measurements performed with the vibrometer. Thus all of the curvature diagrams (independent of whether the curvature is plotted vs. time or temperature) basically show the change in curvature and not the absolute curvature itself.

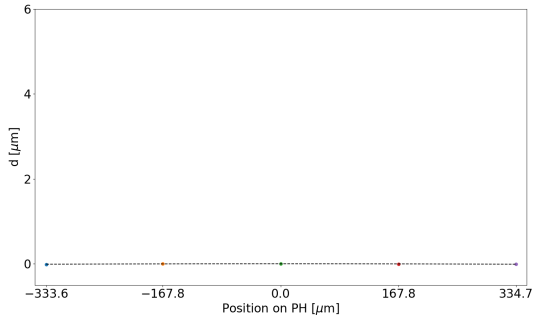

(a) t = 150 ms (start of the power pulse)

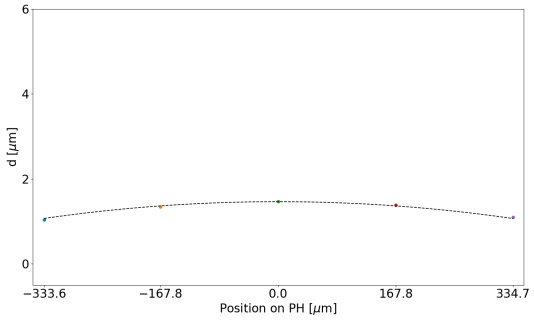

(b) t = 180 ms

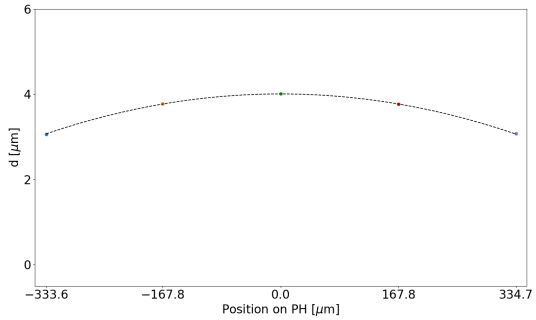

(c) t = 220 ms

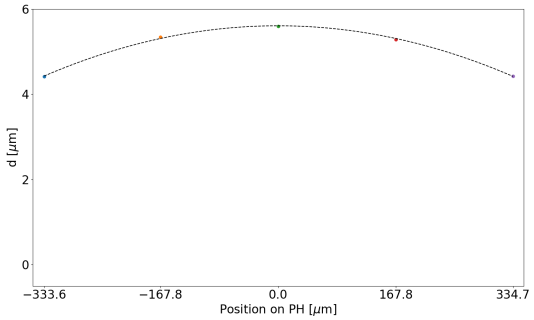

(d) t = 250 ms (end of the heating phase)

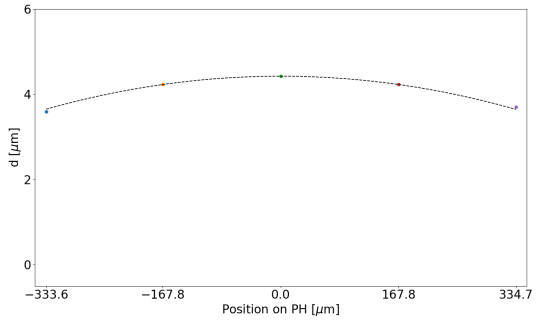

(e) t = 270 ms

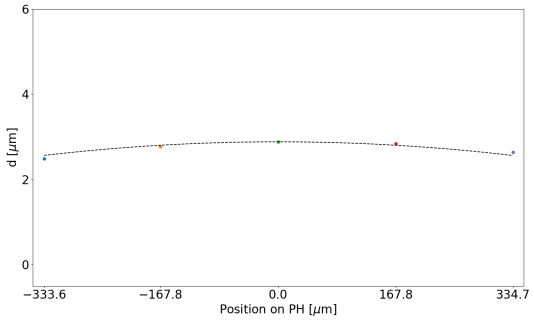

(f) t = 290 ms

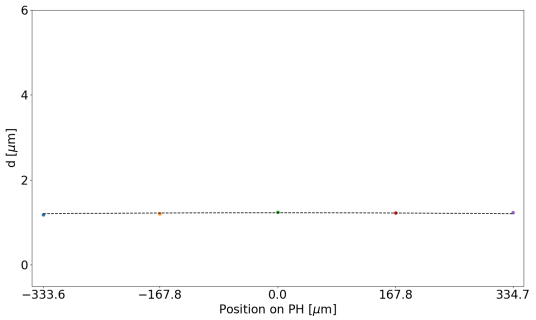

(g) t = 380 ms

Figure 25: Displacements at certain time steps out of fig. 23 including the parabolic fit through the points (black line).

Combining the curvature with the recalculated temperature, also a curvature-temperature curve is obtained (see fig. 26). This representation of the measurement data is common in literature for thermo-mechanical experiments. But as it does not provide any information about the duration or heating rate, it is important to perform all experiments with a constant heating rate to ease the comparison.

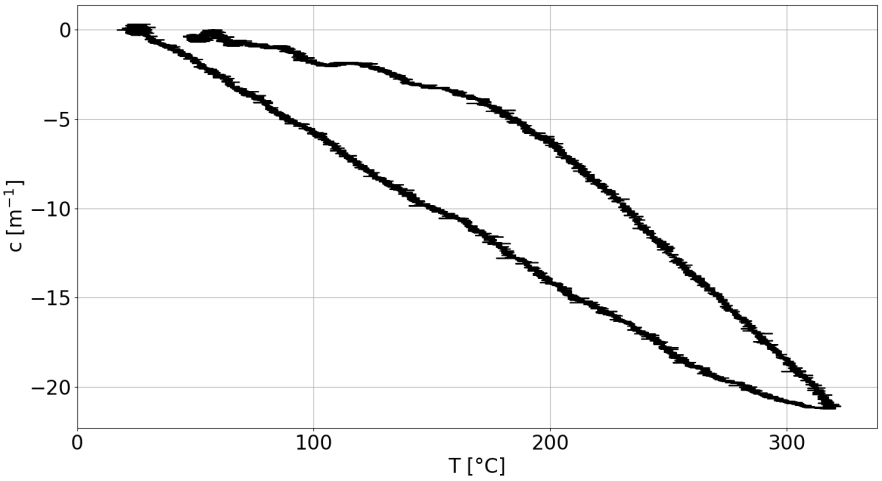

Figure 26: The finally obtained diagram showing curvature vs. temperature for a sample with 60 µm substrate and 20 µm copper thickness and a heating/cooling rate of 3000 K s^{-1}.
T: Temperature in °C; c: Calculated curvature in m^{-1}

4 Results and Discussion

4.1 Optimization of the Measurement

As previously mentioned several settings can be changed in the vibrometer software. This section includes the measurements, which were done to determine the optimal parameters. Basically the most important reason for the optimization is the minimization of the drift and the oscillations of the signal measured. Some of the performed measurements like measurements with different sampling frequencies, measurements, during which the light in the lab was switched on/off or measurements after different waiting times during the heat-up of the He-Ne laser did not affect the result, which is why the diagrams are not included in this thesis. Those measurements and the ones presented in the following two subchapters were performed with a piezoelectric actuator. The advantage of the piezoelectric actuator compared to polyheater samples is, that the piezoelectric actuator can be excited at one of its eigenfrequencies (in our case $f = 82\,\mathrm{kHz}$) leading to well-defined movements of its surface. Because of this the results are very well suited for drawing conclusions in optimizing the setup parameters. The excitation was performed using the internal generator of the setup.

4.1.1 Measurement Range

Figure 27 shows five measurements with different settings of the measurement range of the vibrometer channel. As mentioned the measurements were performed using the piezoelectric actuator meaning that only its vibrational movement should be observed. Instead, those movements are not visible because of the huge drift.

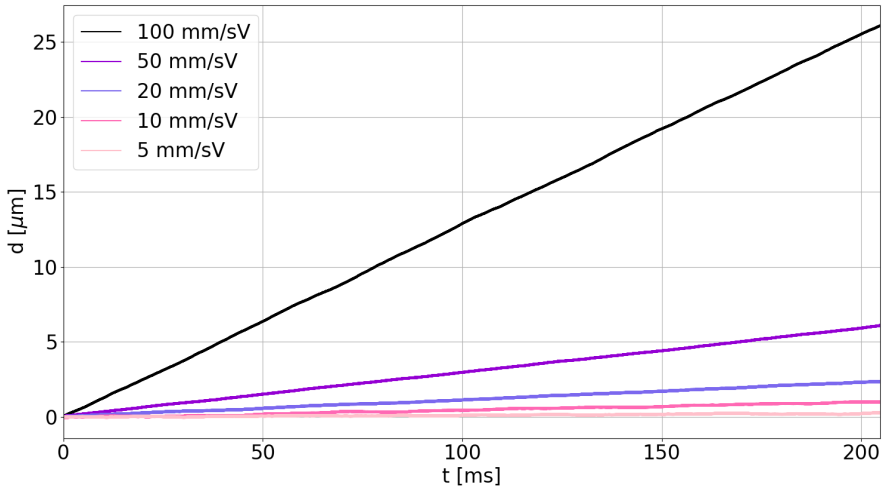

Figure 27: Drift of a sample measured with different measurement ranges.
t: Elapsed time in ms; d: Displacement in µm

For measuring low velocities it is best to choose a low measurement range to decrease the drift as much as possible. But one has to be aware that decreasing the measurement range also decreases the maximum measurable vibration frequency of the sample. This is why the diagram only shows the ranges down to $5\,\mathrm{mm\,s^{-1}\,V^{-1}}$ as the maximum measurable vibration frequency of the sample afterwards falls below 20 kHz, which means that the oscillations of the piezoelectric actuator could not be measured any more.
As typical displacements during a power pulse are in the range of some μm and the vibration frequencies are below 20 kHz, a measurement range of $1\,\mathrm{mm\,s^{-1}\,V^{-1}}$ has been chosen for all the polyheater experiments. This is also the lowest available measurement range that can be selected in the vibrometer software.

4.1.2 Input Voltage

As the measurement range has such a huge impact on the drift, it is best to choose the lowest possible one for all measurements. According to eq. 7, the maximum measurable velocity is given by the product of the measurement range and the input voltage. As the measurement range is kept at $1\,\mathrm{mm\,s^{-1}\,V^{-1}}$, the input voltage has to be increased for measuring higher velocities. Figure 28 shows measurements with different input voltages.

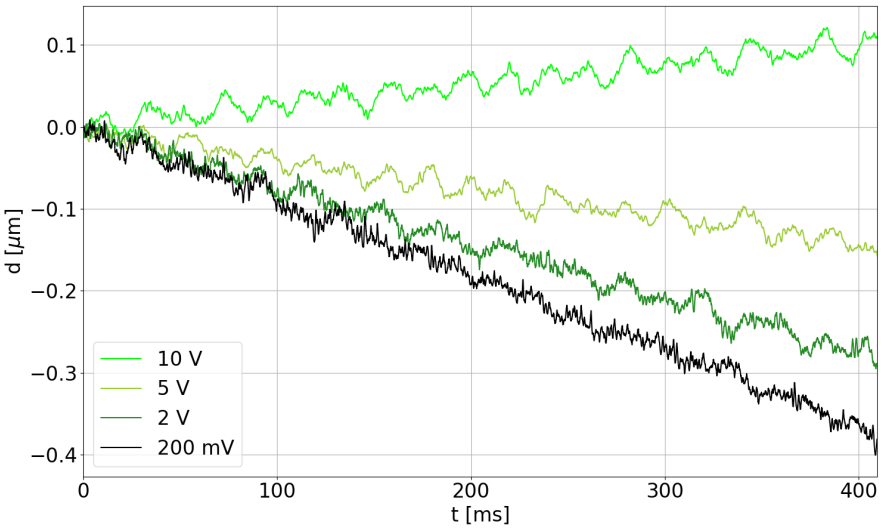

Figure 28: Drift of measurements performed with different input voltages for the vibrometer channel.
t: Elapsed time in ms; d: Displacement in µm

At first glance it looks like high input velocities should be chosen as they have the lowest drift. However, by looking at fig. 28 in more detail, one can see that measurements with input voltages of 200 mV and 2 V show less pronounced oscillations than the ones with higher input voltages (i.e., 5 V and 10 V). As it is easier to correct a linear drift compared to these oscillations, lower input voltages are favourable.

4.1.3 Thinned Polyheaters

It was already mentioned (e.g., sec. 2.1.6 and sec. 3.1.3) that according to Stoney's equation the curvature scales with the square of the substrates thickness. Figure 29 shows a comparison between polyheaters with 120 µm and 60 µm substrate thickness.

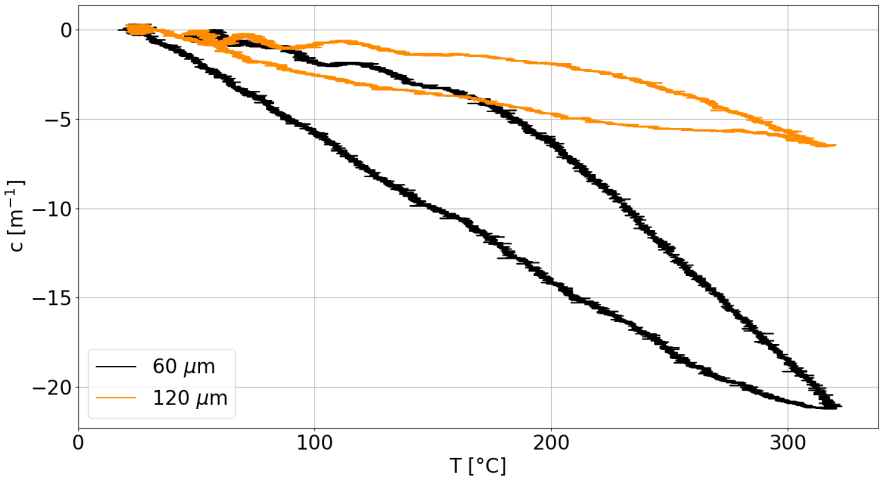

Figure 29: The measured curvatures of a polyheater with a substrate thickness of 60 µm (black) and 120 µm (orange), respectively.
T: Temperature in °C; c: Curvature in m^{-1}

According to eq. 2 reducing the substrate thickness to half of its initial value should result in quadrupling the curvature. But due to the limitations of Stoney's equation, it can only be used as a rough approximation for these samples. In fig. 29 the maximum curvature increased from roughly 6.5 m^{-1} to 21.0 m^{-1} due to the thinning, which is approximately a factor of 3.
Nevertheless one can clearly see that the signal-to-noise ratio is much better for the thinned sample; especially during the cool-down. Because of this, all further measurements were performed on samples with a substrate thickness of 60 µm.

4.1.4 External Vibrations

In sec. 3.2.2 it was already mentioned that the polyheater setup also includes a scanning electron microscope. The pump for the pre-vacuum is placed right next to the table, on which the LSDV is mounted. Basically the table should avoid the impact of vibrations on the measurement but fig. 30 clearly shows that there is still a significant difference based on whether the pump is switched on or off.
This is why the vacuum pump and thus also the scanning electron microscope itself always have to be switched off when performing LSDV measurements. As a consequence, all further measurements presented in this thesis were performed while the pump was being switched off.

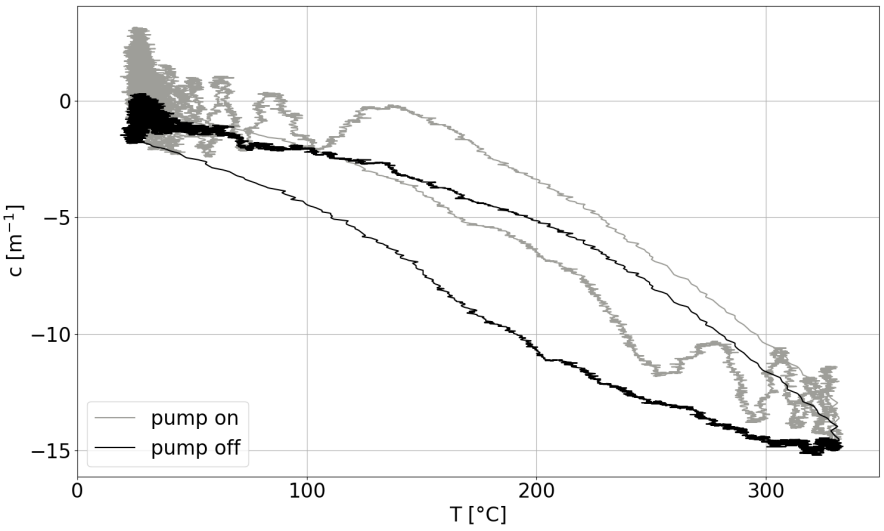

Figure 30: Measured curvature with vacuum pump switched on (grey) and off (black). Note that those measurements were performed with non-linear heating rates.
T: Temperature in °C; c: Curvature in m^{-1}

4.2 Polyheater Measurements

4.2.1 Overview about Measurement Parameters

The following table gives an overview about the chosen parameters for the individual polyheater measurements. The base temperature is not listed in the table as all experiments started at 20 °C, which is the room temperature in the laboratory.

Table 1: Overview of the different parameters for all measurements
h_{Si} ... Thickness of the silicon substrate
T_{max} ... Maximum temperature reached during a pulse
t_{pulse} ... Duration of the pulse applied
V_{in} ... Chosen input range for the vibrometer channel
mr ... Measurement range for the vibrometer channel
v_{max} ... Maximum measurable velocity according to eq. 7

h_{Si} [µm]	T_{max} [°C]	t_{pulse} [ms]	V_{in} [V]	mr [µm s^{-1} V^{-1}]	v_{max} [µm s^{-1}]
60	320	10	1	1000	1000
		100	0.2		200
		1000	0.2		200
	420	13	0.5		500
		100 133	0.2		200
120	320	100	0.2		200

4.2.2 Reproducibility

As the displacement profiles of five points and thus of five temperature pulses on the surface are needed for the curvature calculation, the reproducibility of both, the temperature-time curve as well as the vibrometer measurements is very important.
To check the reproducibility, one single polyheater was pulsed 20 times in a row. During the pulses, the velocity was measured always at the same position on the polyheaters surface. Figure 31 shows the corresponding vibrometer data. The maximum temperature during these pulses varied between 311 °C and 316 °C (also for the first pulse), which is entirely satisfactory. Apart from the first pulse, also the vibrometer measurements can be classified as reproducible. The discrepancy of the first pulse is up to a change in material of the polyheater, not to the vibrometer measurements. In the months between the fabrication and the first measurement, the polyheater has not been cycled, which is why significant room temperature stress relaxation has taken place. During the first pulse strain hardening occurs (see sec. 2.1.2), which is why the displacement curve of the first pulse looks completely different. Afterwards the copper is in a stable state resulting in the following measurements being very similar. This shows that the vibrometer measurements are reproducible, but that some pulses should be performed before the actual measurement to avoid the impact of strain hardening.

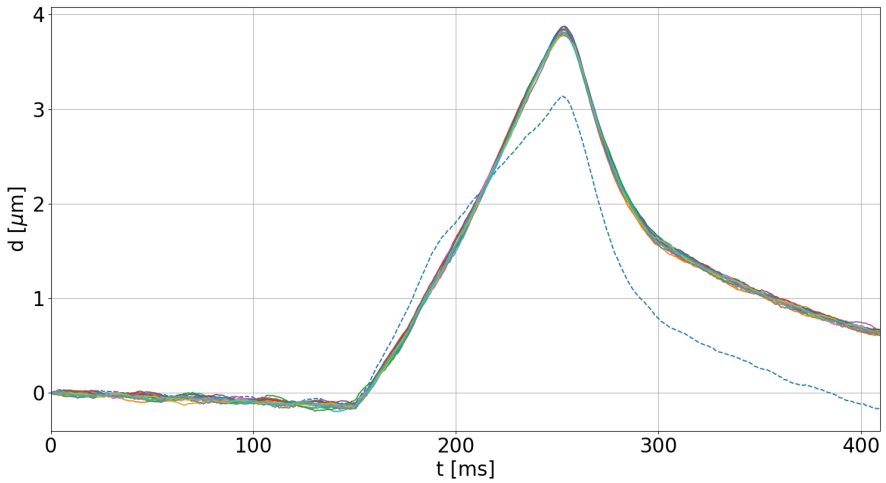

Figure 31: 20 displacement measurements performed with the vibrometer, where the dotted curve represents the first measurement.
t: Time in ms; d: Displacement in µm

4.2.3 Comparison of Different Polyheaters

Figure 32 shows two measurements with the same temperature-time curve performed on different polyheaters. Due to slight differences in the samples, e.g., Cu or poly-silicon thicknesses, an adaptation of the current profile was needed to ensure that both polyheaters reach 420 °C in 100 ms, which equals a heating rate of 4000 K s^{-1}.

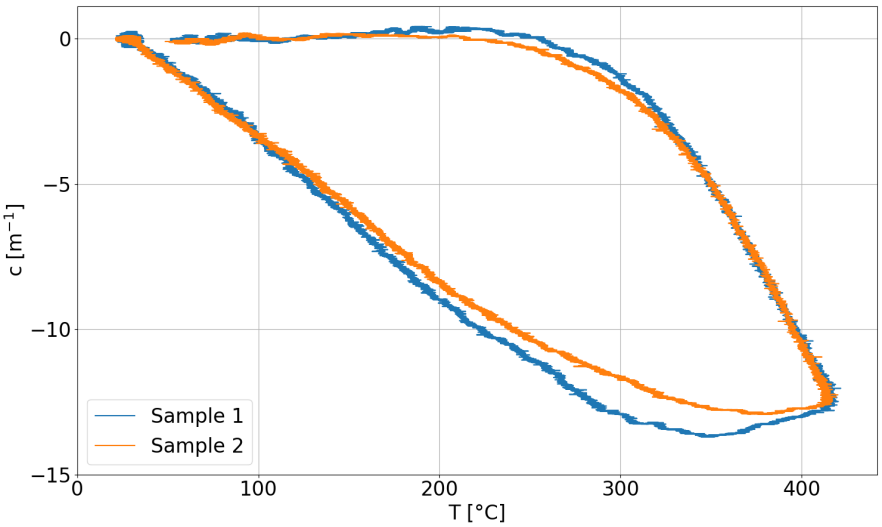

Figure 32: The measured curvature of two different samples showing that different samples give similar results.
T: Temperature in °C; c: Curvature in m^{-1}

Their curvature-temperature relations look relatively similar; especially the slopes during the start of the heating as well as cooling match perfectly. The small deviations, which can be seen during heating at higher temperatures have several possible explanations. One possible cause lies in the thinning process, in particular, in the polishing step. As the polishing machine operates in constant-force mode, it means that the polishing step is non-uniquely defined and for this reason the substrate thickness of the polyheaters may vary within a few micrometers. But as the image of the thinned sample (fig. 13a) shows, the substrate is also a little bit rough and small cracks may have occurred during thinning. Another explanation for the differences is the damage of the temperature sensor. As it is only a thin line (see fig. 11) and the pulses are comparatively long, it damages after a low number of pulses. As often several curvature measurements were performed on one polyheater, the temperature sensor may have been slightly damaged during some of the measurements.

4.2.4 Variation of the Maximum Temperature

The first measurements to investigate the deformation behaviour of a test device were performed up to a temperature of 320 °C. In comparison to wafer curvature measurements performed on wafer pieces (compare fig. 6), they did not show a deviation from the linear-elastic behaviour during heat up. This is why the maximum temperature was increased to 420 °C.
Figure 33 shows a comparison of two pulses with similar heating rates (roughly 3000 $\mathrm{K\,s^{-1}}$) but different pulse durations to reach different maximum temperatures. Now also at high heating rates deviations from the linear-elastic regime occur, but the big difference is the temperature, at which the deviations start. For wafer curvature measurements performed with a heating rate of 0.1 $\mathrm{K\,s^{-1}}$ this already happens at roughly 120 °C (see fig. 6), whereas the vibrometer measurements with high heating rates (3000 $\mathrm{K\,s^{-1}}$) show that it happens above 320 °C.

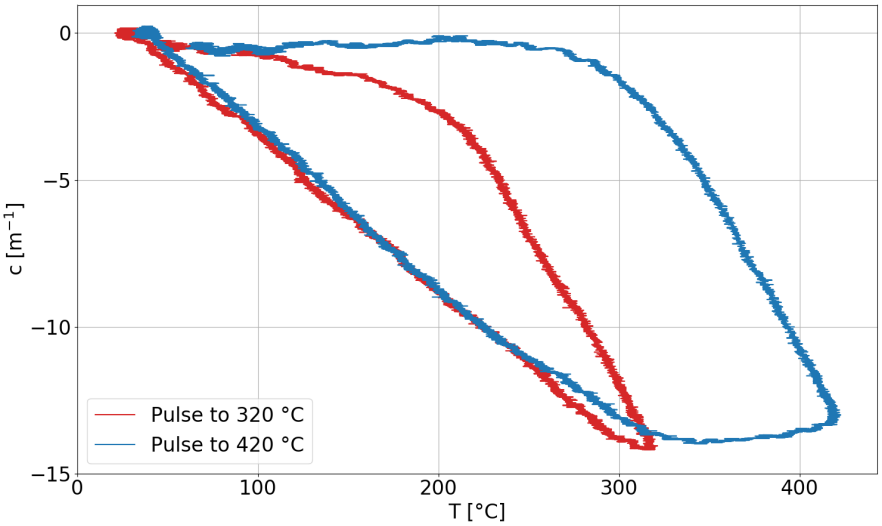

Figure 33: The measured curvature for two different temperature/time curves.
T: Temperature in °C; c: Curvature in $\mathrm{m^{-1}}$

4.2.5 Effect of Different Heating Rates

The final series included three measurements with different heating rates. During all measurements a maximum temperature of 320 °C was reached, but the duration of the applied pulse was varied (10 ms, 100 ms and 1 s) to achieve different heating rates. The corresponding curvatures are plotted in fig. 34. It is remarkable that during heating all the curves show the same behaviour although the heating rate differs by a factor of 100. But during cooling clear differences can be seen: The measurement with the lowest heating rate has the biggest area within the hysteresis curve. This happens because the material has more time for relaxation during the long pulse. For short pulses, the temperature falls very fast meaning that the material can not relax that much.

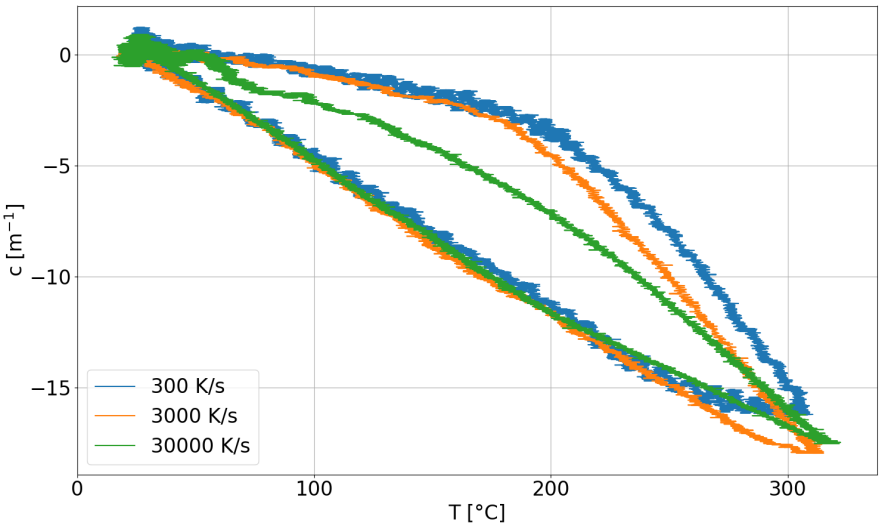

Figure 34: The measured curvature for three different heating rates.
T: Temperature in °C; c: Curvature in m^{-1}

5 Conclusion

To study the thermo-mechanical deformation behaviour of thin films on Si substrates under high heating rates, several parameters of the laser Doppler vibrometer had to be optimized to obtain a better signal-to-noise ratio in the curvature-temperature curves. The most important conclusions, which should be considered for every experiment, are listed in the following (for more details see sec. 4.1):

- Reduction of environmental vibrations, e.g., by switching off the vacuum pump of the scanning electron microscope
- Selection of the lowest possible measurement range
- Selection of the appropriate input voltage according to eq. 7 based on the highest expected velocity

The samples, which are specially designed chips providing active heating, were also "optimized" by reducing the substrate thickness to 60 µm instead of 120 µm using an Allied X-prep system (see sec. 3.1.3 and sec. 4.1.3). For future experiments it would be advisable to use samples, which are directly manufactered with 60 µm substrate thickness, to obtain a more homogeneous and smooth silicon substrate layer. Additionally, samples with a bigger copper surface compared to the ones used for this thesis are going to be manufactured.

In sec. 4.2 the results concerning the polyheater experiments with high heating rates are presented. In the past no such experiments were possible, as the measurement setup had to be extended/improved (see sec. 3.2) to make the measurements of smaller samples possible and a program for analyzing the data had to be written (see sec. 3.4).
The results obtained with the setup including the laser Doppler vibrometer clearly show a significant difference to experiments performed with the (adapted) wafer curvature systems. The most remarkable conclusion from the measurements is that deviations from the linear-elastic regime occur at higher temperatures, if the experiments are performed with higher heating rates (at 320 °C for curvature measurements with a heating rate of $3000\,\mathrm{K\,s^{-1}}$ compared to temperatures around 120 °C for experiments with a heating rate of $0.1\,\mathrm{K\,s^{-1}}$).

The curvature-temperature relations obtained can be used for thermo-mechanically modelling the power metallization layer. For obtaining information about the stress values, FEM simulations are necessary as the approach of using Stoney's equation (calculating the film stress from the curvature data) cannot be applied (see sec. 2.1.6).

Acknowledgements

First and foremost, I want to thank everybody at KAI for the great working environment and for each assistance that everybody of you provided during my work.
Especially I wish to thank "my" group including Manuel Kleinbichler, Sebastian Moser, Michael Reisinger and Johannes Zechner. As Johannes and Sebastian were my supervisors, who guided me during all the time, they deserve my special thanks. I can't think of a better support for all the tasks I had to face!
The following people also deserve to be mentioned explicitly:
Sigrid Göller: The day you showed me everything about the thinning process was great and I am happy that we've met.
Florian Prihbasnik: I really appreciate your help, because without you I would probably still be sitting in front of the computer, writing the python code or waiting for results.
Benjamin Steinwender & Roland Sleik: Thank you very much for your quick help every time I had problems with the ARCTIS system.

I would also like to acknowledge professor Wolfgang Sprengel for his supervision. Thank you for supporting me throughout the whole time and most of all for your quick and helpful solutions/answers to every problem/question I had in mind!

I want to thank my whole family, especially my parents, my sister Christina and my brother-in-law Niki; not only for your support during the time I worked on my thesis but also for the love and encouragement you gave and give me throughout my whole life. Hvala vam za vso vašo pomoč, vašo spodbudo in vaš trud!

Angelika deserves my wholehearted thanks as well. I am truly lucky to count you amongst my friends - thank you for showing so much interest in everything I do. Without your unwavering comfort, motivation and positive talk this thesis and many other things in my life wouldn't have been possible. You are an idol in every sense!

I appreciate and thank Britta; for your caring friendship and help in several situations of my life. Thank you for providing happy distractions to rest my mind outside of my study and for always being there for me.

Additionally I want to express my gratitude to Lara; for your learning and even more your emotional support for the duration of our studies. I am very happy that our time in Graz brought us closer and hope that it stays like this for many more years.

Finally, I want to name professor Antonitsch; your contagious enthusiasm and passion for mathematics had its effect beyond school. Without you I probably neither would have started nor finished studying physics. Thus I would like to express my deepest gratitude.

This work was funded by the Austrian Research Promotion Agency (FFG, Project No. 881110).

References

[1] S. Davis. Back-to-Basics: Power Semiconductors. accessed 16-January-2020, July 2012.

[2] M. Nelhiebel, R. Illing, Th. Detzel, S. Wöhlert, B. Auer, S. Lanzerstorfer, M. Rogalli, W. Robl, S. Decker, J. Fugger, and M. Ladurner. Effective and reliable heat management for power devices exposed to cyclic short overload pulses. *Microelectronics Reliability*, 2013.

[3] S. Moser, G. Zernatto, M. Kleinbichler, M. Nelhiebel, J. Zechner, M. Cordill, and R. Pippan. A Novel Setup for In Situ Monitoring of Thermomechanically Cycled Thin Film Metallizations. *The Journal of the Minerals, Metals & Materials Society*, July 2019.

[4] T. Islam, J. Zechner, M. Bernadoni, M. Nelhiebel, and R. Pippan. A novel setup for wafer curvature measurement at very high heating rates. *Review of Scientific Instruments*, 2017.

[5] P. G. Forrest. *Fatigue of Metals*. Pergamon, Oxford, 1962.

[6] M. F. Ashby. A first report on deformation-mechanism maps. *Acta Metallurgica*, 20(7):887 – 897, 1972.

[7] J. Rösler, H. Harders, and M. Bäker. *Mechanisches Verhalten der Werkstoffe*. Vieweg+Teubner, Wiesbaden, 2008.

[8] O. Kraft, L. B. Freund, R. Phillips, and E. Arzt. Dislocation Plasticity in Thin Metal Films. *MRS Bulletin*, 27:30–37, 2002.

[9] R. W. Hertzberg, R. P. Vinci, and J. L. Hertzberg. *Deformation and Fracture Mechanics of Engineering Materials*. Wiley, Hoboken, 5 edition, 2012.

[10] P. W. J. Oldroyd, D. J. Burns, and P. P. Benham. Paper 2: Strain Hardening and Softening of Metals Produced by Cycles of Plastic Deformation. *Proceedings of the Institution of Mechanical Engineers, Conference Proceedings*, 180(9):392–402, 1965.

[11] M. J. Cordill and T. Schöberl. Script for the lecture "Mechanik in kleinen Dimensionen". 2015.

[12] H. J. Frost and M. F. Ashby. *Deformation-Mechanism Maps: The Plasticity and Creep of Metals and Ceramics*. Pergamon, Cambridge, 1982.

[13] G. G. Stoney. The tension of metallic films deposited by electrolysis. *The Royal Society*, 82:172–175, 1909.

[14] G.C.A.M. Janssen, M.M. Abdalla, F. [van Keulen], B.R. Pujada, and B. [van Venrooy]. Celebrating the 100th anniversary of the Stoney equation for film stress: Developments from polycrystalline steel strips to single crystal silicon wafers. *Thin Solid Films*, 517(6):1858 – 1867, 2009.

[15] R. Huang, C. A. Taylor, S. Himmelsbach, H. Ceric, and T. Detzel. Apparatus for measuring local stress of metallic films, using an array of parallel laser beams during rapid thermal processing. *Measurement Science and Technology*, 21(5), 2010.

[16] T. R. Heidmann. Thermal profilometry for innovative semiconductors. Master's thesis, University of applied sciences Munich, 2018.

[17] Wikipedia. Doppler effect. accessed 17-January-2020, 2019.

[18] Polytec. Vibration Measurement Methods - Laser Doppler Vibrometry. accessed 24-January-2020, 2020.

[19] Wikipedia. Laser Doppler Vibrometer. accessed 24-January-2020, 2019.

[20] T. Aichinger, M. Nelhiebel, S. Einspieler, and T. Grasser. In Situ Poly Heater—A Reliable Tool for Performing Fast and Defined Temperature Switches on Chip. *IEEE Transactions on Device and Materials Reliability*, 10(1):3–8, 2010.

[21] H. Köck, V. Košel, C. Djelassi, M. Glavanovics, and D. Pogany. IR thermography and FEM simulation analysis of on-chip temperature during thermal-cycling power-metal reliability testing using in situ heated structures. *Microelectronics Reliability*, 49(9):1132 – 1136, 2009. 20th European Symposium on the Reliability of Electron Devices, Failure Physics and Analysis.

[22] W. Muth and W. Walter. Bias temperature instability assessment of n- and p-channel MOS transistors using a polysilicon resistive heated scribe lane test structure. *Microelectronics Reliability*, 44(8):1251 – 1262, 2004.

[23] M. Zhang, Y. Yoshihisa, K. Furuya, Y. Imai, K. Hatasako, T. Ipposhi, and S. Maegawa. Reliability study of thermal cycling stress on smart power devices. *Japanese Journal of Applied Physics*, 53(4S), 2014.

[24] T. Smorodin, J. Wilde, P. Alpern, and M. Stecher. Investigation and Improvement of Fast Temperature-Cycle Reliability for DMOS-Related Conductor Path Design. In *2007 IEEE International Reliability Physics Symposium Proceedings. 45th Annual*, pages 486–491, 2007.

[25] H. V. Nguyen, C. Salm, J. Vroemen, J. Voets, B. Krabbenborg, J. Bisschop, A. J. Mouthaan, and F. G. Kuper. Test chip for detecting thin film cracking induced by fast temperature cycling and electromigration in multilevel interconnect systems. In *Proceedings of the 9th International Symposium on the Physical and Failure Analysis of Integrated Circuits*, pages 135–139, 2002.

[26] M. Nelhiebel, R. Illing, C. Schreiber, S. Wöhlert, S. Lanzerstorfer, M. Ladurner, C. Kadow, S. Decker, D. Dibra, H. Unterwalcher, M. Rogalli, W. Robl, T. Herzig, M. Poschgan, M. Inselsbacher, M. Glavanovics, and S. Fraissé. A reliable technology concept for active power cycling to extreme temperatures. *Microelectronics Reliability*, 2011.

[27] Allied High Tech Products. *X-PREP Product Information Guide*.

[28] Polytec. *Polytec Scanning Vibrometer, Hardware Handbuch*, 2012.